J. Fluid Mech. (1990), *vol.* 221, *pp.* 205–232
Printed in Great Britain

An angular spectrum model for propagation of Stokes waves

By KYUNG DUCK SUH†, ROBERT A. DALRYMPLE AND JAMES T. KIRBY

Center for Applied Coastal Research, Department of Civil Engineering, University of Delaware, Newark, DE 19716, USA

(Received 15 August 1989)

An angular spectrum model for predicting the transformation of Stokes waves on a mildly varying topography is developed, including refraction, diffraction, shoaling and nonlinear wave interactions. The equations governing the water-wave motion are perturbed using the method of multiple scales and Stokes expansions for the velocity potential and free-surface displacement. The first-order solution is expressed as an angular spectrum, or directional modes, of the wave field propagating on a beach with straight iso-baths whose depth is given by laterally averaged depths. The equations for the evolution of the angular spectrum due to the effects of bottom variation and cubic resonant interaction are obtained from the higher-order problems. Comparison of the present model with existing models is made for some simple cases. Numerical examples of the time-independent version of the model are presented for laboratory experiments for wave diffraction behind a breakwater gap and wave focusing over submerged shoals: an elliptic shoal on a sloping beach and a circular shoal on a flat bottom.

1. Introduction

Since Booker & Clemmow (1950) clarified the concept of the angular spectrum of plane waves, it has been applied in various branches of physics and engineering that deal with wave propagation (see Ratcliffe 1956; Gabor 1961; Clemmow 1966). In water-wave-propagation problems, Stamnes *et al.* (1983) used an angular spectrum model to study wave focusing by a lens in water of constant depth. Recently Dalrymple & Kirby (1988) developed an angular spectrum model for propagation of linear water waves on a beach with straight and parallel bottom contours. This model was extended to the case of irregular bathymetry by Dalrymple *et al.* (1989). These models are solved by a marching method starting from given wave data offshore and give accurate results for waves propagating at large angles from the assumed propagation direction (positive x-direction in this paper) if the bottom variation in the y-direction is not severe.

The governing equation in the models of Dalrymple & Kirby (1988) and Dalrymple *et al.* (1989) is the linear mild-slope equation developed by Berkhoff (1972). Dalrymple *et al.* incorporated nonlinearity in the model by correcting the wave parameters iteratively using an empirical nonlinear dispersion relationship proposed by Kirby & Dalrymple (1986). In the present study, we develop an angular spectrum model for the propagation of Stokes waves over a mildly-varying topography,

† Present address: Virginia Institute of Marine Science, Gloucester Point, VA 23062, USA.

including nonlinearity in a more rigorous fashion. In §2, a simple angular spectrum model for water of constant depth is derived, illustrating the angular spectrum and its physical significance. In §3, the equations governing the water-wave motion are perturbed using the method of multiple scales and Stokes expansions for the velocity potential and free-surface displacement, yielding a set of perturbation equations at each order in wave steepness. In §4, the first- and second-order problems are solved completely and a set of equations governing the slow evolution of the angular spectrum is obtained. In §5, we explore some subsets of the equations derived in §4 and they are compared with some existing models. Numerical examples to show the ability of the model are presented in §6, and finally a summary of the main results of the paper is given in §7.

2. The angular spectrum and its physical interpretation

In order to illustrate the concept of the angular spectrum and its physical significance, we consider the Helmholtz equation in $\Phi(x,y)$ in water of constant depth:

$$\frac{\partial^2 \Phi}{\partial x^2}+\frac{\partial^2 \Phi}{\partial y^2}+k^2\Phi = 0, \tag{2.1}$$

where k is the constant wavenumber and the complex wave potential $\Phi(x,y)$ is related to the total velocity potential for the wave motion, $\phi(x, y, z, t)$, by

$$\phi = \Phi(x, y)\cosh k(h+z)\,\mathrm{e}^{-\mathrm{i}\omega t}, \tag{2.2}$$

where $\mathrm{i} = \sqrt{-1}$, ω is the angular frequency of the wave, h is the constant water depth, and the vertical coordinate z is measured vertically upwards from the still-water line.

Suppose that a wave field represented by $\Phi(0, y)$ is incident on the line $x = 0$, propagating into the half-plane $x > 0$. The Fourier transform of $\Phi(0,y)$ in the y-direction is

$$\hat{\Phi}(0,\lambda) = \int_{-\infty}^{\infty} \Phi(0,y)\,\mathrm{e}^{-\mathrm{i}\lambda y}\,\mathrm{d}y, \tag{2.3}$$

where the circumflex denotes a transformed variable and λ is the continuous Fourier parameter. The inverse Fourier transform is

$$\Phi(0,y) = \frac{1}{2\pi}\int_{-\infty}^{\infty} \hat{\Phi}(0,\lambda)\,\mathrm{e}^{\mathrm{i}\lambda y}\,\mathrm{d}\lambda. \tag{2.4}$$

Noting that the unit-amplitude plane wave propagating in the direction of $\boldsymbol{k} \equiv ((k^2-\lambda^2)^{\frac{1}{2}}, \lambda)$ is $\exp[\mathrm{i}((k^2-\lambda^2)^{\frac{1}{2}}x+\lambda y)]$, $\exp(\mathrm{i}\lambda y)$ may be regarded as a unit-amplitude plane wave propagating in that direction at $x = 0$. The complex amplitude of that plane-wave component is simply $(1/2\pi)\hat{\Phi}(0,\lambda)\,\mathrm{d}\lambda$ as can be seen in (2.4). For this reason, $\hat{\Phi}(0,\lambda)$ is called the *angular spectrum* of the wave field $\Phi(0,y)$. The angular spectrum is merely the Fourier transform of a wave field along a straight line, each component of which represents the complex amplitude of the plane wave propagating in a certain direction.

The Fourier transform of (2.1) in the y-direction provides an equation for the evolution of the angular spectrum $\hat{\Phi}(x,\lambda)$:

$$\hat{\Phi}_{xx}+(k^2-\lambda^2)\hat{\Phi} = 0, \tag{2.5}$$

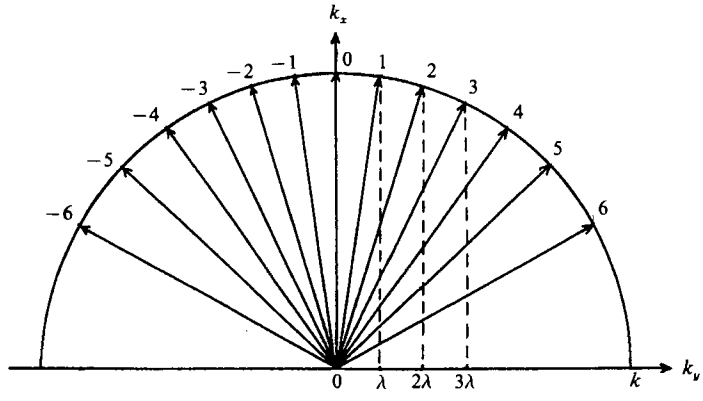

FIGURE 1. Diagram of the Fourier decomposition of the wave field on a row with an angular spectrum (with lateral wavenumbers, $p\lambda$, $p = 0, \pm 1, \pm 2, \ldots$). k_x and k_y are the wavenumbers in the x- and y-directions, respectively.

where subscripts denote partial differentiation. An elementary solution to this equation for constant k is

$$\hat{\Phi}(x, \lambda) = \hat{\Phi}(0, \lambda) \exp\left[\mathrm{i}\,(k^2 - \lambda^2)^{\frac{1}{2}} x\right]. \tag{2.6}$$

This result will be interpreted differently depending on the magnitude of $(k^2 - \lambda^2)$. If $(k^2 - \lambda^2) > 0$, then the effect of propagation over a distance x is simply a change in the relative phases of the various components of the angular spectrum. Since each plane-wave component propagates at a different angle, each travels a different distance to reach a given observation point and relative phase delays are thus introduced. If $(k^2 - \lambda^2) < 0$, these wave components decay exponentially as they propagate in the x-direction. Such components of the angular spectrum are called *evanescent modes*. The limiting case, $(k^2 - \lambda^2) = 0$, corresponds to the plane wave propagating in the y-direction, contributing no net energy flow in the x-direction.

Finally, the inverse Fourier transform of (2.6) gives the solution to (2.1) in terms of the initial angular spectrum $\hat{\Phi}(0, \lambda)$:

$$\Phi(x, y) = \frac{1}{2\pi} \int_{-\infty}^{\infty} \hat{\Phi}(0, \lambda) \exp\left[\mathrm{i}\,(k^2 - \lambda^2)^{\frac{1}{2}} x\right] \exp\left[\mathrm{i}\lambda y\right] \mathrm{d}\lambda. \tag{2.7}$$

This equation implies that it is sufficient to know the free-surface displacement on the line $x = 0$ to determine it at any point in the half-plane $x > 0$. Note, however, that this is an approximate solution comprised of plane waves only. Though (2.7) is the exact solution to the Helmholtz equation (2.1), it is not the full solution of the linearized water-wave problem on constant depth, which would include all of the vertical eigenmodes. In fact, as shown in Stamnes (1986), one must know the velocity potential in the plane $x = 0$ for all values of y and for all z-values between the bottom at $z = -h$ and the undisturbed water surface at $z = 0$. The full solution of the linearized problem is given in § 19.1 of Stamnes (1986) along with a discussion of the range of validity of the approximate solution in (2.7) of the present paper.

In the actual computation using discrete data values on a computational grid, a discrete Fourier transform is used under the assumption that the model domain is periodic in the y-direction. By discretizing the domain of width l by $N+1$ equidistant

points of spacing $\Delta y = l/N$ so that $\Phi(x,0) = \Phi(x, N\Delta y)$, the velocity potential $\Phi(x,y)$ defined on the first N points can be transformed into discrete Fourier modes by

$$\hat{\Phi}(x,p) = \frac{1}{N}\sum_{j=0}^{N-1} \Phi(x,j\Delta y)\,\mathrm{e}^{-\mathrm{i}p\lambda j\Delta y} \quad (p = 0, \pm 1, \pm 2, \ldots, \pm(\tfrac{1}{2}N-1), -\tfrac{1}{2}N), \tag{2.8}$$

which describe the wave components propagating in different directions as indicated in figure 1. The inversion formula is

$$\Phi(x,j\Delta y) = \sum_{p} \hat{\Phi}(x,p)\,\mathrm{e}^{\mathrm{i}p\lambda j\Delta y} \quad (j = 0, 1, 2, \ldots, (N-1)), \tag{2.9}$$

where

$$\lambda = \frac{2\pi}{N\Delta y}, \tag{2.10}$$

which is different from the continuous Fourier parameter λ used previously. These transforms can be performed efficiently by using a fast Fourier transform.

3. Governing equations and multiple-scale perturbation expansions

The exact equations governing the velocity potential $\phi(x, y, z, t)$ and the free surface $\eta(x, y, t)$ of the waves propagating in water of finite depth, assuming incompressible fluid and irrotational flow motion, are given by

$$\nabla^2\phi = 0 \quad (-h < z < \eta), \tag{3.1}$$

$$g\phi_z + \phi_{tt} + |\nabla\phi|_t^2 + \tfrac{1}{2}(\nabla\phi\cdot\nabla)|\nabla\phi|^2 = 0 \quad (z = \eta), \tag{3.2}$$

$$\phi_t + \tfrac{1}{2}|\nabla\phi|^2 + g\eta = 0 \quad (z = \eta), \tag{3.3}$$

$$\phi_z = -\nabla_{\mathrm{h}}\phi\cdot\nabla_{\mathrm{h}}h \quad (z = -h), \tag{3.4}$$

where ∇ and ∇_{h} are the three-dimensional and horizontal gradient operators, respectively, g is the gravitational acceleration, and $h(x,y)$ is the water depth measured from the still-water line.

The method of multiple scales has been proven to be a powerful tool for problems of weakly nonlinear waves by Benney & Roskes (1969), Yue & Mei (1980), and Kirby & Dalrymple (1983), among others. In the present multiple-scale analysis we introduce the following slow variables:

$$x_1 = \epsilon x, \quad x_2 = \epsilon^2 x, \ldots; \; t_1 = \epsilon t, \quad t_2 = \epsilon^2 t, \ldots, \tag{3.5}$$

where ϵ is the Stokes-wave steepness parameter, so that the derivatives with respect to x and t are replaced by

$$\frac{\partial}{\partial x} \sim \frac{\partial}{\partial x} + \epsilon\frac{\partial}{\partial x_1} + \epsilon^2\frac{\partial}{\partial x_2} + \ldots; \quad \frac{\partial}{\partial t} \sim \frac{\partial}{\partial t} + \epsilon\frac{\partial}{\partial t_1} + \epsilon^2\frac{\partial}{\partial t_2} + \ldots, \tag{3.6}$$

where x and t relate to the fast wave-like characteristics while $x_1, x_2, \ldots$, and $t_1, t_2, \ldots$, cover the slower modulation of the wave field.

No assumption is made yet for scales for y since the lateral variation of the wave field will be taken care of later by its angular spectrum representation, which therefore makes it possible to model the large-angle components and the small-angle components of the wave field equally well (cf. figure 1). This differs from previously derived models in which appropriate scaling for y was also made depending on the problem to be considered. In the parabolic models of Yue & Mei (1980) and Kirby & Dalrymple (1983), for example, they chose two scales x and x_2 in the x-direction, while in the y-direction only one variable, $y_1 = \epsilon y$, was chosen under the assumption that no fast wavelike variation occurs in the y-direction, consistent with the

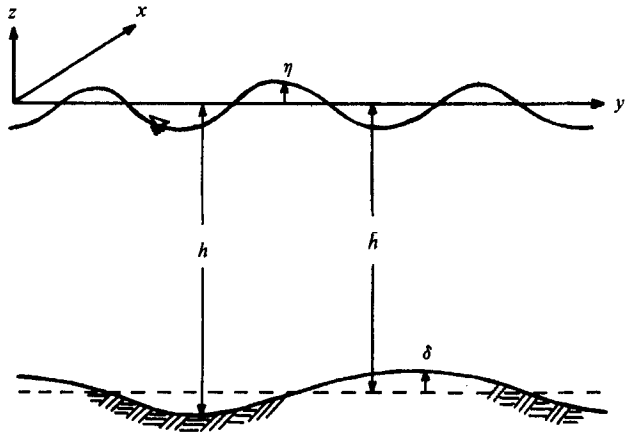

FIGURE 2. Definition of depth components.

parabolic approximation, but the effect of finite angles of propagation with respect to the x-axis allows the amplitude to vary in the y-direction $O(\epsilon^{-1})$ times faster than in the x-direction.

The bottom boundary condition (3.4) is defined for different water depths at different locations in the y-direction. For its angular spectrum representation, however, we need to express it for a reference depth which is constant in the y-direction. This is chosen, in this study, as the laterally averaged depth, $\bar{h}$, given by

$$\bar{h}(x) = \frac{1}{l}\int_0^l h(x,y)\,\mathrm{d}y, \tag{3.7}$$

so that

$$h(x,y) = \bar{h}(1-\nu), \tag{3.8}$$

where

$$\nu(x,y) = \frac{\delta(x,y)}{\bar{h}(x)}. \tag{3.9}$$

Here $\delta(x,y)$ is the deviation of the actual bottom from the laterally averaged depth, as indicated in figure 2. Note that $\bar{h}$ is a function of x only and the variability of depth in the y-direction is contained in $\nu(x,y)$, whose magnitude is usually much smaller than unity if the topography does not deviate greatly from straight and parallel contours.

In order to determine the point at which the effect of bottom slope and bottom irregularity (in the y-direction) enters the bottom boundary condition, we need to choose the scales for $\nabla_{\mathrm{h}} h$ and $\nu(x,y)$. Assuming mildly-varying topography, we restrict $\nabla_{\mathrm{h}} h$ to be $O(\epsilon^2)$, that is,

$$h_x \approx \epsilon^2 h_{x_2}, \quad h_y \approx \epsilon^2 h_{y_2}, \tag{3.10}$$

where an additional scale, $y_2 \sim \epsilon^2 y$, was defined. Accordingly, we assume

$$\bar{h}_x \approx \epsilon^2 \bar{h}_{x_2}, \quad \delta_x \approx \epsilon^2 \delta_{x_2}, \quad \delta_y \approx \epsilon^2 \delta_{y_2}. \tag{3.11}$$

The bottom is then effectively locally flat up to the third order in ϵ. These scales for bottom slopes were chosen by Djordjević & Redekopp (1978) and Kirby & Dalrymple (1983). With this choice the effect of bottom slope becomes as important as the nonlinearities; that is, both the bottom-slope terms and the cubic nonlinear terms appear first in the equations at third order.

For the magnitude of the lateral bottom irregularities, we assume $\nu \approx O(\epsilon)$ so that

$$\delta(x, y) = \epsilon \bar{h} \mu(x, y), \tag{3.12}$$

where $\mu(x, y) \approx O(1)$ is introduced for later convenience. The effect of lateral bottom irregularities then appears at the second order in ϵ. This scale necessitates the choice of the slow variables x_1 and t_1 which are omitted in Yue & Mei (1980) and Kirby & Dalrymple (1983) based on the argument that for Stokes waves the modulation scales in horizontal space and time are $O(\epsilon^{-2})$ times greater than the wavelength and wave period, respectively. Without these slow variables, the ϕ_{21} problem in §4.2 becomes unsolvable since it is then identical to the homogeneous first-order problem except for the inhomogeneous bottom boundary condition. The bottom forcing term in the second-order problem is introduced by the process of modifying the actual bottom boundary condition (3.4) to one on the laterally averaged depth. In the models of Yue & Mei and Kirby & Dalrymple, this process is not necessary and the ϕ_{21} problem is identical to the first-order problem, so they neglected the solution for ϕ_{21}. If we assumed $\nu \approx O(\epsilon^2)$, this difficulty could be avoided; the bottom topography, however, then could be assumed as straight and parallel contours.

We proceed by expanding the free-surface conditions (3.2) and (3.3) about $z = 0$ and the bottom boundary condition (3.4) about $z = -\bar{h}(x)$ in Taylor series. Substitution of Stokes expansions for ϕ and η:

$$\phi = \sum_{n=1}^{\infty} \epsilon^n \phi_n, \quad \eta = \sum_{n=1}^{\infty} \epsilon^n \eta_n, \tag{3.13}$$

into these equations, with the scales (3.6), (3.10)–(3.12), then gives a boundary-value problem in z for each order of n:

$$\nabla^2 \phi_n = F_n \quad (-\bar{h} < z < 0), \tag{3.14}$$

$$g\phi_{n_z} + \phi_{n_{tt}} = G_n \quad (z = 0), \tag{3.15}$$

$$\phi_{n_t} + g\eta_n = H_n \quad (z = 0), \tag{3.16}$$

$$\phi_{n_z} = B_n \quad (z = -\bar{h}), \tag{3.17}$$

where F_n, G_n, H_n, B_n are the forcing terms determined by lower-order solutions and are given in the Appendix.

4. Evolution of the angular spectrum

The boundary value problems (3.14)–(3.17) are solved up to the second order in order to obtain the third-order forcing terms which describe the cubic nonlinear interaction. The first-order solution is expressed in terms of the angular spectrum. Since the higher-order problems are linear in ϕ_n, the method of superposition allows the solution in the form, $\phi_n = \phi_{n1} + \phi_{n2} + \ldots + \phi_{nn}$, where ϕ_{n1} is the waves proportional to the first harmonics, ϕ_{n2} is the sum and difference waves, and so forth. Then since the problem of ϕ_{n1} is inhomogeneous and its homogeneous version (i.e. the first-order problem) has ϕ_1 as a non-trivial solution, they must satisfy a solvability condition, which follows by applying Green's second identity to ϕ_1 and ϕ_{n1} and leads to the so-called evolution equations governing the slow modulation of the angular spectrum.

4.1. *First-order solution*

For $n = 1$, the problem (3.14)–(3.17) is homogeneous, and describes waves propagating on a beach with straight and parallel bottom contours whose depth is given by $\bar{h}(x)$. The solutions for ϕ_1 and η_1 can be readily obtained in the form of the discrete Fourier transform (cf. equation (2.9)) as

$$\phi_1 = \sum_p \left(-\frac{ig}{2\omega} f A_p \, e^{i\psi_p} + \text{c.c.} \right), \quad \eta_1 = \sum_p \left(\tfrac{1}{2} A_p \, e^{i\psi_p} + \text{c.c.} \right), \tag{4.1}$$

where c.c. is the complex conjugate, ψ_p is the phase function:

$$\psi_p = \int^x (k^2 - (p\lambda)^2)^{\frac{1}{2}} \, dx + p\lambda y - \omega t, \tag{4.2}$$

in which λ is given by (2.10), and the angular frequency ω is related to the laterally averaged depth, $\bar{h}(x)$, and the corresponding wavenumber $\bar{k}(x)$ (hereafter we use $k \equiv \bar{k}$ for simplicity) by

$$\omega^2 = gk \tanh k\bar{h}. \tag{4.3}$$

$A_p(x_1, x_2, t_1, t_2)$ is the slowly varying complex amplitude of the wave component propagating in the direction $\boldsymbol{k} = ((k^2 - (p\lambda)^2)^{\frac{1}{2}}, p\lambda)$, and

$$f = \frac{\cosh k(\bar{h} + z)}{\cosh k\bar{h}}. \tag{4.4}$$

The index p varying from $-\frac{1}{2}N$ to $(\frac{1}{2}N - 1)$ (cf. equation (2.8)) describes the plane wave components propagating in different directions as indicated in figure 1. The wave components for which $(p\lambda)^2 > k^2$ represent the evanescent modes which decay exponentially in the x-direction. Since in general k has the minimum value at the offshore boundary, some evanescent modes become progressive modes as they propagate into shallower region. In this study, these evanescent modes are neglected and only the progressive modes at the offshore boundary are carried into the domain, assuming the energy of the evanescent modes is negligibly small compared with that of the progressive modes. We close this section by mentioning that $k_x \approx \epsilon^2 k_{x_2}$ and $f_x = \epsilon^2 f_{x_2}$ since we assumed $\bar{h}_x$ to be $O(\epsilon^2)$.

4.2. *Second-order solution*

Since the second-order problem is linear in ϕ_2 and η_2, it can be advantageously solved by assuming

$$\phi_2 = \phi_{21} + \phi_{22}, \quad \eta_2 = \eta_{21} + \eta_{22}, \tag{4.5}$$

in which ϕ_{21} and η_{21} are taken to satisfy the problem with the forcing terms proportional to the first harmonics (i.e. $\exp(\pm i\psi_p)$), while ϕ_{22} and η_{22} satisfy the problem with the remaining forcing terms proportional to $\exp[\pm i(\psi_q \pm \psi_r)]$. The indices q, r, varying from $-\frac{1}{2}N$ to $(\frac{1}{2}N - 1)$, correspond to the index p in (4.2).

Assuming ϕ_{21} and η_{21} to have the forms

$$\phi_{21} = \sum_p [(\phi_{21})_p \, e^{i\Omega_p} e^{ip\lambda y} + \text{c.c.}], \quad \eta_{21} = \sum_p [(\eta_{21})_p \, e^{i\Omega_p} e^{ip\lambda y} + \text{c.c.}], \tag{4.6}$$

where

$$\Omega_p = \int^x (k^2 - (p\lambda)^2)^{\frac{1}{2}} \, dx - \omega t, \tag{4.7}$$

and recalling the formula for inverse discrete Fourier transform (2.9), we observe that $(\phi_{21})_p \exp(i\Omega_p)$, $p = 0, \pm 1, \ldots$, represent the discrete Fourier components of ϕ_{21} without its conjugate part. Expressing the forcing terms in the same form as (4.6), for example,

$$F_{21} = \sum_p [(F_{21})_p e^{i\Omega_p} e^{ip\lambda y} + \text{c.c.}], \tag{4.8}$$

the discrete Fourier transform of the ϕ_{21} problem, omitting the conjugate part and dividing through by $\exp(i\Omega_p)$, is given by

$$\left(\frac{\partial^2}{\partial z^2} - k^2\right)(\phi_{21})_p = (F_{21})_p \quad (-\bar{h} < z < 0), \tag{4.9}$$

$$g\frac{\partial}{\partial z}(\phi_{21})_p - \omega^2(\phi_{21})_p = (G_{21})_p \quad (z = 0), \tag{4.10}$$

$$-i\omega(\phi_{21})_p + g(\eta_{21})_p = (H_{21})_p \quad (z = 0), \tag{4.11}$$

$$\frac{\partial}{\partial z}(\phi_{21})_p = (B_{21})_p \quad (z = -\bar{h}). \tag{4.12}$$

Before proceeding to solve this problem, we need the evolution equation for A_p at the second order. By letting

$$\phi_1 = \sum_p [(\phi_{11})_p e^{i\Omega_p} e^{ip\lambda y} + \text{c.c.}], \tag{4.13}$$

the boundary-value problem for $(\phi_{11})_p$ is the homogeneous form of the equations (4.9)–(4.12). Applying Green's second identity to $(\phi_{11})_p$ and $(\phi_{21})_p$, we obtain the solvability condition

$$\int_{-\bar{h}}^{0} (F_{21})_p f \, dz = \frac{1}{g}(G_{21})_p - \frac{(B_{21})_p}{\cosh k\bar{h}}. \tag{4.14}$$

Performing the integration over depth and noting that

$$\int_{-\bar{h}}^{0} f^2 \, dz = \frac{CC_g}{g}, \tag{4.15}$$

where $C = \omega/k$, $C_g = \partial\omega/\partial k$, leads to the evolution equation for A_p

$$A_{p_{t_1}} = -\frac{(k^2 - (p\lambda)^2)^{\frac{1}{2}}}{k} C_g A_{p_{x_1}} + \frac{i\omega k\bar{h}}{\sinh 2k\bar{h}} e^{-i\Theta_p} I_p^1, \tag{4.16}$$

where

$$\Theta_p = \int^x (k^2 - (p\lambda)^2)^{\frac{1}{2}} dx, \tag{4.17}$$

and

$$I_p^1 = F_p[\mu(x, y) F^{-1}(A_m e^{i\Theta_m})] \tag{4.18}$$

represents the forcing due to the interaction between surface wave modes and lateral bottom variation. F^{-1} and F_p on the right-hand side denote the inverse Fourier transform and the pth component of the discrete Fourier transform, respectively. The superscript 1 in I_p^1 is used because other wave–bottom interaction terms of the similar form will appear later. Each mode of the angular spectrum, A_p, thus can be modified at the second order through the interaction of surface waves with the lateral bottom variation. On straight and parallel contours, the wave–bottom interaction

term I_p^1 vanishes since $\mu(x, y) = 0$ everywhere. The effect of bottom slope has not entered yet at the second order. Without the wave–bottom interaction term, (4.16) describes the wave envelope A_p propagating without change of form on a locally flat bottom at the speed $((k^2-(p\lambda)^2)^{\frac{1}{2}}/k)C_g$ in the x-direction which is the x-component of the group velocity C_g.

The solution for $(\phi_{21})_p$ is obtained by using the method of variation of parameters as

$$(\phi_{21})_p = -\frac{g}{2\omega}\frac{(k^2-(p\lambda)^2)^{\frac{1}{2}}}{k}(\bar{h}+z)\frac{\sinh k(\bar{h}+z)}{\cosh k\bar{h}}A_{p_{x_1}} + \tfrac{1}{2}\mathrm{i}\omega\bar{h}\frac{\sinh k(\bar{h}+z)}{\sinh k\bar{h}}\mathrm{e}^{-\mathrm{i}\theta_p}I_p^1. \quad (4.19)$$

The corresponding free-surface displacement $(\eta_{21})_p$ is

$$(\eta_{21})_p = -\frac{\mathrm{i}}{2\omega}\frac{(k^2-(p\lambda)^2)^{\frac{1}{2}}}{k}(C_g+\omega\bar{h}\tanh k\bar{h})A_{p_{x_1}} + \frac{k\bar{h}(2\sinh^2 k\bar{h}-1)}{2\sinh 2k\bar{h}}\mathrm{e}^{-\mathrm{i}\theta_p}I_p^1. \quad (4.20)$$

The solution for the sum and difference waves is given, as in Sharma & Dean (1979), by

$$\phi_{22} = \sum_q\sum_r [C_{qr}^+ f_{qr}^+ A_q A_r \mathrm{e}^{\mathrm{i}(\psi_q+\psi_r)} + C_{qr}^- f_{qr}^- A_q A_r^* \mathrm{e}^{\mathrm{i}(\psi_q-\psi_r)}] + \text{c.c.}, \quad (4.21)$$

$$\eta_{22} = \sum_q\sum_r [D_{qr}^+ A_q A_r \mathrm{e}^{\mathrm{i}(\psi_q+\psi_r)} + D_{qr}^- A_q A_r^* \mathrm{e}^{\mathrm{i}(\psi_q-\psi_r)}] + \text{c.c.}, \quad (4.22)$$

where * also denotes the complex conjugate and

$$C_{qr}^{\pm} = \frac{\Gamma_{qr}^{\pm}}{gk_{qr}^{\pm}\tanh k_{qr}^{\pm}\bar{h}-(\omega\pm\omega)^2}, \quad (4.23)$$

$$D_{qr}^{\pm} = \frac{1}{g}[\Delta_{qr}^{\pm} + \mathrm{i}(\omega\pm\omega)C_{qr}^{\pm}], \quad (4.24)$$

$$\Gamma_{qr}^{\pm} = \pm\frac{\mathrm{i}g^2}{2\omega}((k^2-(q\lambda)^2)^{\frac{1}{2}}(k^2-(r\lambda)^2)^{\frac{1}{2}} + (q\lambda)(r\lambda) \mp \tfrac{3}{2}R^2 \pm \tfrac{1}{2}k^2), \quad (4.25)$$

$$\Delta_{qr}^{\pm} = -\frac{g^2}{8\omega^2}((k^2-(q\lambda)^2)^{\frac{1}{2}}(k^2-(r\lambda)^2)^{\frac{1}{2}} + (q\lambda)(r\lambda) \mp R^2 - 2R^2), \quad (4.26)$$

$$R = k\tanh k\bar{h} = \frac{\omega^2}{g}, \quad (4.27)$$

$$f_{qr}^{\pm} = \frac{\cosh k_{qr}^{\pm}(\bar{h}+z)}{\cosh k_{qr}^{\pm}\bar{h}}, \quad (4.28)$$

$$k_{qr}^{\pm} = |\boldsymbol{k}_q \pm \boldsymbol{k}_r|, \quad (4.29)$$

$$\boldsymbol{k}_q = (k^2-(q\lambda)^2)^{\frac{1}{2}}\boldsymbol{i} + (q\lambda)\boldsymbol{j}, \quad (4.30)$$

where $\boldsymbol{i}$ and $\boldsymbol{j}$ are the unit vectors in the x- and y-directions, respectively. It can be shown for the case of a single wavetrain that this solution reduces to that of Stokes second-order theory, i.e.

$$\phi_{22}(q=r) = -\tfrac{3}{16}\mathrm{i}\omega\frac{\cosh 2k(\bar{h}+z)}{\sinh^4 k\bar{h}}A_q\mathrm{e}^{2\mathrm{i}\psi_q} + \text{c.c.} \quad (4.31)$$

4.3. *Evolution equations for the angular spectrum* A_s

For $n = 3$, again the problem is linear in ϕ_3 so that we can separate the solution as $\phi_3 = \phi_{31} + \phi_{32} + \phi_{33}$ as in the second-order problem. Neglecting the forcing terms, F_{32}, G_{32} and B_{32}, representing quadratic resonances which can occur only in shallow water, and expressing ϕ_{31} as

$$\phi_{31} = \sum_s [(\phi_{31})_s \, e^{i\Omega_s} e^{is\lambda y} + \text{c.c.}], \tag{4.32}$$

the discrete Fourier transform of the ϕ_{31} problem, without its conjugate part, is given by

$$\left(\frac{\partial^2}{\partial z^2} - k^2\right)(\phi_{31})_s \, e^{i\Omega_s} = (F_{31})_s \, e^{i\Omega_s} \qquad (-\bar{h} < z < 0), \tag{4.33}$$

$$g\frac{\partial}{\partial z}(\phi_{31})_s \, e^{i\Omega_s} - \omega^2(\phi_{31})_s \, e^{i\Omega_s} = (G_{31})_s \, e^{i\Omega_s} + (G_{33})_s \qquad (z = 0), \tag{4.34}$$

$$\frac{\partial}{\partial z}(\phi_{31})_s \, e^{i\Omega_s} = (B_{31})_s \, e^{i\Omega_s} \qquad (z = -\bar{h}). \tag{4.35}$$

The forcing terms, $(F_{31})_s$, $(G_{31})_s$, and $(B_{31})_s$, are obtained from the third-order forcing terms directly proportional to the first harmonics, and the cubic resonant interaction term $(G_{33})_s$ due to the interactions between the primary waves and the sum and difference waves or among the primary waves themselves is

$$(G_{33})_s = \sum_p \sum_q \sum_r Q A_p A_q A_r^* \exp[i(\Omega_p + \Omega_q - \Omega_r)]\delta_{s=p+q-r}, \tag{4.36}$$

where the interaction coefficient Q is given by

$$\begin{aligned}
Q = &-g[(k^2-(r\lambda)^2)^{\frac{1}{2}}((k^2-(q\lambda)^2)^{\frac{1}{2}} - (k^2-(p\lambda)^2)^{\frac{1}{2}})\,(r\lambda)\,(q\lambda + p\lambda) \\
&- Rk_{qp}^{+}\tanh(k_{qp}^{+}\bar{h}) + \tfrac{1}{2}k_{qp}^{+2}]\,C_{qp}^{+} - \frac{ig^2}{2\omega}(k^2 - R^2)(D_{qp}^{+} - D_{qr}^{-} - D_{rq}^{-*}) \\
&- \frac{i}{8}\frac{g^3}{\omega^3}[(k^2-(p\lambda)^2)^{\frac{1}{2}}(k^2-(q\lambda)^2)^{\frac{1}{2}}(k^2-(r\lambda)^2)^{\frac{1}{2}}(2(k^2-(p\lambda)^2)^{\frac{1}{2}} - (k^2-(r\lambda)^2)^{\frac{1}{2}}) \\
&+ (p\lambda)(q\lambda)(r\lambda)(2(p\lambda) - (r\lambda)) + k^2R^2 + 2(k^2-(p\lambda)^2)^{\frac{1}{2}}(k^2-(r\lambda)^2)^{\frac{1}{2}}(q\lambda)\,(p\lambda - r\lambda) \\
&+ 2(k^2-(p\lambda)^2)^{\frac{1}{2}}(k^2-(q\lambda)^2)^{\frac{1}{2}}(q\lambda)(r\lambda) - 4R^2((k^2-(p\lambda)^2)^{\frac{1}{2}}(k^2-(r\lambda)^2)^{\frac{1}{2}} + (p\lambda)\,(r\lambda)) \\
&- 2R^2((k^2-(p\lambda)^2)^{\frac{1}{2}}(k^2-(q\lambda)^2)^{\frac{1}{2}} + (p\lambda)\,(q\lambda))],
\end{aligned} \tag{4.37}$$

and the Kronecker delta, $\delta_{s=p+q-r}$, describing the resonant condition has the value 1 if $s = p+q-r$ is satisfied and is 0 otherwise. For the self-interaction of a single wavetrain ($p = q = r = s$), this reduces to

$$Q = \tfrac{1}{2}ig\omega k^2 \frac{\cosh 4k\bar{h} + 8 - 2\tanh^2 k\bar{h}}{8\sinh^4 k\bar{h}}, \tag{4.38}$$

which is the coefficient of the cubic nonlinear term in the nonlinear Schrödinger equations of Yue & Mei (1980) and Kirby & Dalrymple (1983).

Again applying Green's second identity to $(\phi_{31})_s e^{i\Omega_s}$ and $(\phi_{11})_s e^{i\Omega_s}$, we obtain the solvability condition

$$\int_{-\bar{h}}^{0} (F_{31})_s f \, dz = \frac{1}{g}[(G_{31})_s + (G_{33})_s e^{-i\Omega_s}] - \frac{(B_{31})_s}{\cosh k\bar{h}}, \tag{4.39}$$

which leads to the evolution equation for A_s at the third order:

$$\begin{aligned} &A_{s_{t_2}} + \frac{(k^2-(s\lambda)^2)^{\frac{1}{2}}}{k} C_g A_{s_{x_2}} + \frac{[(k^2-(s\lambda)^2)^{\frac{1}{2}} CC_g]_{x_2}}{2\omega} A_s + iD_s A_{s_{x_1x_1}} \\ &+ \frac{\bar{h}(k^2-(s\lambda)^2)^{\frac{1}{2}}}{\sinh 2k\bar{h}} (\tfrac{1}{2}C_g + \omega\bar{h}\tanh k\bar{h}) e^{-i\Theta_s} I_s^5 \\ &+ \frac{\bar{h}}{\sinh 2k\bar{h}} (\tfrac{1}{2}C_g + (2C_g - C)\sinh^2 k\bar{h} - 2C) e^{-i\Theta_s} I_s^2 \\ &- \frac{i\omega k^2\bar{h}^2}{2\sinh^2 2k\bar{h}} (1 + 4\sinh^2 k\bar{h}) e^{-i\Theta_s} I_s^6 \\ &- \frac{g}{2\omega\cosh^2 k\bar{h}} e^{-i\Theta_s}(I_s^3 + I_s^4) + \frac{1}{g}(G_{33})_s e^{-i\Omega_s} = 0, \end{aligned} \tag{4.40}$$

where

$$D_s = \frac{k^2-(s\lambda)^2}{k^2}\left(\frac{C_g^2}{2\omega} + C_g\bar{h}\tanh k\bar{h}\right) - \frac{C_g}{2k} - \frac{g(k^2-(s\lambda)^2)}{4\omega k^2}\left(\bar{h} + \bar{h}\tanh^2 k\bar{h} - \frac{\tanh k\bar{h}}{k}\right), \tag{4.41}$$

and the new wave–bottom interaction terms are

$$I_s^2 = F_s[\mu(x,y) F^{-1}((k^2-(m\lambda)^2)^{\frac{1}{2}} A_{m_{x_1}} e^{i\Theta_m})], \tag{4.42}$$

$$I_s^3 = F_s[\delta_{x_2} F^{-1}((k^2-(m\lambda)^2)^{\frac{1}{2}} A_m e^{i\Theta_m})], \tag{4.43}$$

$$I_s^4 = F_s[\delta_{y_2} F^{-1}((m\lambda) A_m e^{i\Theta_m})], \tag{4.44}$$

$$I_s^5 = F_s[\mu(x,y) F^{-1}(A_{m_{x_1}} e^{i\Theta_m})], \tag{4.45}$$

$$I_s^6 = F_s[\mu^2 F^{-1}(A_m e^{i\Theta_m})]. \tag{4.46}$$

Adding (4.16) with s instead of p and ϵ times the equation (4.40), considering A_s as functions of x_1 and t_1 only, that is,

$$\frac{\partial}{\partial t_1} + \epsilon\frac{\partial}{\partial t_2} \longrightarrow \frac{\partial}{\partial t_1}, \quad \frac{\partial}{\partial x_1} + \epsilon\frac{\partial}{\partial x_2} \longrightarrow \frac{\partial}{\partial x_1}, \tag{4.47}$$

yield

$$\begin{aligned} &A_{s_{t_1}} + \frac{(k^2-(s\lambda)^2)^{\frac{1}{2}}}{k} C_g A_{s_{x_1}} + \epsilon\frac{[(k^2-(s\lambda)^2)^{\frac{1}{2}} CC_g]_{x_2}}{2\omega} A_s + i\epsilon D_s A_{s_{x_1x_1}} - \frac{i\omega k\bar{h}}{\sinh 2k\bar{h}} e^{-i\Theta_s} I_s^1 \\ &+ \epsilon\frac{\bar{h}(k^2-(s\lambda)^2)^{\frac{1}{2}}}{\sinh 2k\bar{h}} (\tfrac{1}{2}C_g + \omega\bar{h}\tanh k\bar{h}) e^{-i\Theta_s} I_s^5 + \epsilon\frac{\bar{h}}{\sinh 2k\bar{h}} (\tfrac{1}{2}C_g + (2C_g - C)\sinh^2 k\bar{h} \\ &- 2C) e^{-i\Theta_s} I_s^2 - \epsilon\frac{i\omega k^2\bar{h}^2}{2\sinh^2 2k\bar{h}} (1 + 4\sinh^2 k\bar{h}) e^{-i\Theta_s} I_s^6 \\ &- \epsilon\frac{g}{2\omega\cosh^2 k\bar{h}} e^{-i\Theta_s}(I_s^3 + I_s^4) + \frac{\epsilon}{g}(G_{33})_s e^{-i\Omega_s} = 0. \end{aligned} \tag{4.48}$$

Using the scales, $\partial/\partial t_1 \approx \epsilon^{-1}(\partial/\partial t)$, $\partial/\partial x_1 \approx \epsilon^{-1}(\partial/\partial x)$, $\partial/\partial x_2 \approx \epsilon^{-2}(\partial/\partial x)$, $\mu \approx \epsilon^{-1}\nu$, $\delta_{x_2} \approx \epsilon^{-2}\delta_x$, $\delta_{y_2} \approx \epsilon^{-2}\delta_y$, finally we obtain the evolution equation for A_s in the physical coordinates (x, y, t):

$$
\begin{aligned}
&A_{s_t} + \frac{(k^2-(s\lambda)^2)^{\frac{1}{2}}}{k} C_g A_{s_x} + \frac{[(k^2-(s\lambda)^2)^{\frac{1}{2}} CC_g]_x}{2\omega} A_s + iD_s A_{s_{xx}} \\
&- \frac{i\omega k\bar{h}}{\sinh 2k\bar{h}} e^{-i\theta_s} F_s[\nu F^{-1}(A_m e^{i\theta_m})] \\
&+ \frac{\bar{h}(k^2-(s\lambda)^2)^{\frac{1}{2}}}{\sinh 2k\bar{h}} (\tfrac{1}{2}C_g + \omega\bar{h}\tanh k\bar{h}) e^{-i\theta_s} F_s[\nu F^{-1}(A_{m_x} e^{i\theta_m})] \\
&+ \frac{\bar{h}}{\sinh 2k\bar{h}} (\tfrac{1}{2}C_g + (2C_g - C)\sinh^2 k\bar{h} - 2C) e^{-i\theta_s} F_s[\nu F^{-1}((k^2-(m\lambda)^2)^{\frac{1}{2}} A_{m_x} e^{i\theta_m})] \\
&- \frac{i\omega k^2\bar{h}^2}{2\sinh^2 2k\bar{h}} (1 + 4\sinh^2 k\bar{h}) e^{-i\theta_s} F_s[\nu^2 F^{-1}(A_m e^{i\theta_m})] \\
&- \frac{g e^{-i\theta_s}}{2\omega\cosh^2 k\bar{h}} F_s[\delta_x F^{-1}((k^2-(m\lambda)^2)^{\frac{1}{2}} A_m e^{i\theta_m}) + \delta_y F^{-1}((m\lambda) A_m e^{i\theta_m})] \\
&+ \frac{1}{g}(G_{33})_s e^{-i\Omega_s} = 0.
\end{aligned}
\tag{4.49}
$$

The ordering parameter ϵ was removed from the last term since it has served its purpose. This equation governs the slow evolution of the wave component A_s due to refraction, diffraction, shoaling, and nonlinear wave interactions. The third term represents the shoaling/refraction of each wave component on laterally averaged depth. The complicated periodic convolution terms represent wave diffraction due to the interaction between surface wave and the lateral bottom variation, which disappear on straight and parallel contours, and the last term involving $(G_{33})_s$ contains the cubic nonlinearities.

The time-dependent equation (4.49) is of parabolic type. This equation represents a very general approach to the solution of wave propagation in a domain with properly posed initial condition (at $t = 0$) and boundary conditions (at $x = 0$ and $x = b$ where b is the length of the domain in the x-direction). In many practical applications, however, the assumption of steadiness of the wave field may be appropriately utilized. The time-independent equation for A_s cannot be obtained simply by dropping the first term in (4.49) since the time dependency of A_s was extensively involved in deriving other terms. One may obtain it by setting the derivatives with respect to the slow times t_1 and t_2 to be zero from the outset and repeating the derivation. The resulting expression for the time-independent evolution equations for A_s is

$$
\begin{aligned}
&\frac{(k^2-(s\lambda)^2)^{\frac{1}{2}}}{k} C_g A_{s_x} + \frac{[(k^2-(s\lambda)^2)^{\frac{1}{2}} CC_g]_x}{2\omega} A_s - i\frac{\omega k\bar{h}}{\sinh 2k\bar{h}} e^{-i\theta_s} F_s[\nu F^{-1}(A_m e^{i\theta_m})] \\
&+ i\frac{\omega^2 k^4 \bar{h}^2}{C_g^2 (k^2-(s\lambda)^2)^{\frac{1}{2}} \sinh^2 2k\bar{h}} E_s e^{-i\theta_s} F_s\left[\nu F^{-1}\left\{\frac{1}{(k^2-(m\lambda)^2)^{\frac{1}{2}}} F_m[\nu F^{-1}(A_n e^{i\theta_n})]\right\}\right] \\
&- i\frac{\omega k^2\bar{h}^2}{C_g \sinh 2k\bar{h}}\left(\tfrac{1}{2}C\tanh k\bar{h} + \frac{g}{\omega\cosh^2 k\bar{h}}\right) e^{-i\theta_s} F_s[\nu^2 F^{-1}(A_m e^{i\theta_m})]
\end{aligned}
$$

$$-\frac{g\,\mathrm{e}^{-\mathrm{i}\Theta_s}}{2\omega\cosh^2 k\bar{h}}F_s[\delta_x F^{-1}((k^2-(m\lambda)^2)^{\frac{1}{2}}A_m\,\mathrm{e}^{\mathrm{i}\Theta_m})+\delta_y F^{-1}((m\lambda)A_m\,\mathrm{e}^{\mathrm{i}\Theta_m})]$$

$$+\frac{1}{g}(G_{33})_s\,\mathrm{e}^{-\mathrm{i}\Omega_s}=0, \tag{4.50}$$

where
$$E_s=\frac{1}{2}\left[\frac{C_g}{k}+\frac{g(k^2-(s\lambda)^2)}{2\omega k^2}\left(\bar{h}+\bar{h}\tanh^2 k\bar{h}-\frac{\tanh k\bar{h}}{k}\right)\right]. \tag{4.51}$$

The angular spectrum A_s is now phase-shifted by the substitution

$$A_s=A'_s\exp[\mathrm{i}((k_0^2-(s\lambda)^2)^{\frac{1}{2}}x-\int^x(k^2-(s\lambda)^2)^{\frac{1}{2}}\mathrm{d}x)], \tag{4.52}$$

where k_0 is a fixed reference wavenumber at $x=0$ (the offshore boundary). A'_s is then the angular spectrum of the velocity potential ϕ_1 given by

$$\phi_1=\sum_s\left(-\frac{\mathrm{i}g}{2\omega}fA'_s\exp[\mathrm{i}((k_0^2-(s\lambda)^2)^{\frac{1}{2}}x+s\lambda y-\omega t)]+\text{c.c.}\right). \tag{4.53}$$

By this procedure, we can eliminate the integral of the wavenumber component in the x-direction,

$$\int^x(k^2-(s\lambda)^2)^{\frac{1}{2}}\mathrm{d}x,$$

which introduces errors when it is computed numerically. Substituting (4.52) into (4.50) and multiplying through by $k/((k^2-(s\lambda)^2)^{\frac{1}{2}}C_g)$ gives

$$\begin{aligned}
A'_{s_x}=\;&\mathrm{i}((k^2-(s\lambda)^2)^{\frac{1}{2}}-(k_0^2-(s\lambda)^2)^{\frac{1}{2}})A'_s-\frac{[(k^2-(s\lambda)^2)^{\frac{1}{2}}CC_g]_x}{2(k^2-(s\lambda)^2)^{\frac{1}{2}}CC_g}A'_s\\
&+\mathrm{i}\frac{\omega k^2\bar{h}}{C_g(k^2-(s\lambda)^2)^{\frac{1}{2}}\sinh 2k\bar{h}}\mathrm{e}^{-\mathrm{i}\Theta'_s}F_s[\nu F^{-1}(A'_m\,\mathrm{e}^{\mathrm{i}\Theta'_m})]\\
&-\mathrm{i}\frac{\omega^2k^5\bar{h}^2}{C_g^3(k^2-(s\lambda)^2)\sinh^2 2k\bar{h}}E_s\,\mathrm{e}^{-\mathrm{i}\Theta'_s}F_s\left[\nu F^{-1}\left\{\frac{1}{(k^2-(m\lambda)^2)^{\frac{1}{2}}}F_m[\nu F^{-1}(A'_n\,\mathrm{e}^{\mathrm{i}\Theta'_n})]\right\}\right]\\
&+\mathrm{i}\frac{\omega k^3\bar{h}^2}{C_g(k^2-(s\lambda)^2)^{\frac{1}{2}}\sinh 2k\bar{h}}\left(\tfrac{1}{2}C\tanh k\bar{h}+\frac{g}{\omega\cosh^2 k\bar{h}}\right)\mathrm{e}^{-\mathrm{i}\Theta'_s}F_s[\nu^2F^{-1}(A'_m\,\mathrm{e}^{\mathrm{i}\Theta'_m})]\\
&+\frac{g\mathrm{e}^{-\mathrm{i}\Theta'_s}}{2CC_g(k^2-(s\lambda)^2)^{\frac{1}{2}}\cosh^2 k\bar{h}}F_s[\delta_x F^{-1}((k^2-(m\lambda)^2)^{\frac{1}{2}}A'_m\,\mathrm{e}^{\mathrm{i}\Theta'_m})\\
&+\delta_y F^{-1}((m\lambda)A'_m\,\mathrm{e}^{\mathrm{i}\Theta'_m})]-\frac{k}{gC_g(k^2-(s\lambda)^2)^{\frac{1}{2}}}(G_{33})'_s\,\mathrm{e}^{-\mathrm{i}\Omega'_s}(s=0,\ \pm1,\ \pm2,\dots),
\end{aligned} \tag{4.54}$$

where
$$\Theta'_s=(k_0^2-(s\lambda)^2)^{\frac{1}{2}}x, \tag{4.55}$$

$$(G_{33})'_s=\sum_p\sum_q\sum_r QA'_pA'_qA'^*_r\exp[\mathrm{i}(\Omega'_p+\Omega'_q-\Omega'_r)]\,\delta_{s-p+q-r}, \tag{4.56}$$

$$\Omega'_s=\Theta'_s-\omega t. \tag{4.57}$$

Equation (4.54) is coupled nonlinear first-order ordinary differential equations for $A'_s, s=0,\ \pm1,\dots$, which can be solved by standard numerical methods provided

initial conditions for A_s' at $x = 0$ (offshore boundary) are specified. In this study, we use the fourth-order Runge–Kutta method. The details of finite-differencing and stability analysis of the numerical method are in Suh (1989).

5. Comparison with previously derived models for some simple cases

In this section, we explore the correspondences of our evolution equations to previously derived models.

5.1. *Time-dependent models*

5.1.1. *Evolution of wave envelopes propagating normal to shore on a beach with straight and parallel contours*

Djordjević & Redekopp (1978) derived an evolution equation for wave envelopes propagating normal to shore (positive x-direction in this study) on a beach with straight iso-baths. Simplification of the evolution equation (4.48) to this case can be made by setting $s = 0$ ($A = A_0$), dropping all the wave–bottom interaction terms, and using the scales $\partial/\partial t_1 \approx \epsilon(\partial/\partial t_2)$ and $\partial/\partial x_1 \approx \epsilon(\partial/\partial x_2)$, to yield

$$A_{t_2} + C_g A_{x_2} + \frac{[kCC_g]_{x_2}}{2\omega} A - \tfrac{1}{2}\mathrm{i}\epsilon^2 \frac{\partial^2 \omega}{\partial k^2} A_{x_2 x_2} + \mathrm{i}K|A|^2 A = 0, \tag{5.1}$$

where

$$D_s(s=0) = \frac{C_g^2}{2\omega} + C_g h \tanh kh - \frac{\omega h \cosh^2 kh}{k \sinh 2kh} = -\frac{1}{2}\frac{\partial^2 \omega}{\partial k^2} \tag{5.2}$$

was used and

$$K = \omega k^2 \frac{\cosh 4kh + 8 - 2\tanh^2 kh}{16 \sinh^4 kh}. \tag{5.3}$$

On a constant depth, the third term in (5.1) disappears and the equation reduces to the two-dimensional version of Davey & Stewartson (1974) equation without the term representing the effect of first-order long waves, which were omitted in the present study.

By introducing the following variables:

$$\tau = \epsilon\left[\int^x \frac{\mathrm{d}x}{C_g(\xi)} - t\right] = \epsilon^{-1}\int^\xi \frac{\mathrm{d}\xi}{C_g(\xi)} - \epsilon^{-1} t_2, \tag{5.4}$$

$$\xi = \epsilon^2 x = x_2, \tag{5.5}$$

into (5.1) as in Djordjević & Redekopp (1978), we obtain, after neglecting the terms of $O(\epsilon)$ or smaller, the evolution equation for $A(\xi, \tau)$ as

$$2\mathrm{i}\omega C_g A_\xi + \mathrm{i}[kCC_g]_\xi A + \frac{\omega}{C_g^2}\frac{\partial^2 \omega}{\partial k^2} A_{\tau\tau} - 2\omega K|A|^2 A = 0. \tag{5.6}$$

In the notation of Djordjević & Redekopp, this equation can be written as

$$2\mathrm{i}\omega C_g A_\xi - \mathrm{i}g\sigma \frac{k_\xi}{k}(1 - kh\sigma) A - \left\{1 - \frac{gh}{C_g^2}(1 - kh\sigma)(1 - \sigma^2)\right\} A_{\tau\tau} - \frac{gk^3}{8\sigma}\left(\frac{9}{\sigma^2} - 12 + 13\sigma^2 - 2\sigma^4\right)|A|^2 A = 0, \tag{5.7}$$

where $\sigma = \tanh kh$. Except for some algebraic differences in the last term, this equation is identical to Djordjević & Redekopp equation without the term involving long waves. The fourth term in their equation is dimensionally incorrect.

5.1.2. *Resonant interactions between two trains of deep-water gravity waves*

Following the analysis of Phillips (1960) for the growth of a tertiary wave by the resonant interaction among three primary waves, Longuet-Higgins (1962) studied the resonant interaction between two trains of deep-water gravity waves which is a simpler case of the three-wave interaction when two of the three primary waves are identical. Studies for the nonlinear evolution of wave envelopes due to cubic resonances were also made in parallel. Based on the work of Benney & Newell (1967), Roskes (1976*a*) presented a nonlinear Schrödinger equation system of the following form to describe the slowly varying amplitudes of two deep-water waves:

$$A_{1_T}+\boldsymbol{C}_{g_1}\cdot\nabla_h A_1-i\epsilon\sum_{i,j}\gamma_{1_{ij}}\frac{\partial^2 A_1}{\partial X_i\,\partial X_j}-i\epsilon A_1[\beta_{11}|A_1|^2+\beta_{12}|A_2|^2]=0, \tag{5.8}$$

$$A_{2_T}+\boldsymbol{C}_{g_2}\cdot\nabla_h A_2-i\epsilon\sum_{i,j}\gamma_{2_{ij}}\frac{\partial^2 A_2}{\partial X_i\,\partial X_j}-i\epsilon A_2[\beta_{21}|A_1|^2+\beta_{22}|A_2|^2]=0, \tag{5.9}$$

where $T=\epsilon t$, $\boldsymbol{X}=\epsilon\boldsymbol{x}$, β_{ij} is the interaction coefficients, and the dispersion tensors $\gamma_{l_{ij}}$, $l=1,2$, are defined by

$$\gamma_{l_{ij}}=\frac{1}{2}\frac{\partial^2}{\partial k_i\,\partial k_j}\omega(\boldsymbol{k}_l). \tag{5.10}$$

For an angular spectrum which varies only in the x-direction, (5.8) and (5.9) can be simplified by dropping the terms involving the derivative of the amplitude with respect to X_2 which corresponds to the y-direction in our notation. If we consider two components of an angular spectrum, each propagating in directions $\boldsymbol{k}_m=(k^2-(m\lambda)^2)^{\frac{1}{2}}\boldsymbol{i}+(m\lambda)\boldsymbol{j}$ and $\boldsymbol{k}_n=(k^2-(n\lambda)^2)^{\frac{1}{2}}\boldsymbol{i}+(n\lambda)\boldsymbol{j}$ with the same frequency ω, (5.8) and (5.9) can be written in the present notation as

$$A_{m_{t_1}}+\frac{(k^2-(m\lambda)^2)^{\frac{1}{2}}}{k}C_g A_{m_{x_1}}+i\epsilon D_m A_{m_{x_1x_1}}-i\epsilon A_m[\beta_{11}|A_m|^2+\beta_{12}|A_n|^2]=0, \tag{5.11}$$

$$A_{n_{t_1}}+\frac{(k^2-(n\lambda)^2)^{\frac{1}{2}}}{k}C_g A_{n_{x_1}}+i\epsilon D_n A_{n_{x_1x_1}}-i\epsilon A_n[\beta_{21}|A_m|^2+\beta_{22}|A_n|^2]=0, \tag{5.12}$$

which are equivalent to (4.48) in deep water. For this case, Roskes (1976*b*) gave the interaction coefficients β_{ij} as

$$\beta_{11}=\beta_{22}=-\tfrac{1}{2}\omega k^2, \tag{5.13}$$

$$\beta_{12}=\beta_{21}=-\omega k|\boldsymbol{k}_m+\boldsymbol{k}_n|\sin^2\tfrac{1}{2}\theta-4\omega k^2|\boldsymbol{k}_m+\boldsymbol{k}_n|\sin^2\tfrac{1}{2}\theta\sin^2\tfrac{1}{2}\phi/(|\boldsymbol{k}_m+\boldsymbol{k}_n|-4k)$$
$$+2\omega k^2\sin^2\tfrac{1}{2}\theta-\omega k^2(\sin^2\tfrac{1}{2}\theta\cos^2\tfrac{1}{2}\theta+1), \tag{5.14}$$

where θ is the angle between $\boldsymbol{k}_m$ and $\boldsymbol{k}_n$, and ϕ is the angle between $-\boldsymbol{k}_m$ and $(\boldsymbol{k}_m+\boldsymbol{k}_n)$ as indicated in figure 3. Comparing the cubic nonlinear terms in (4.48) and (5.11), it can be shown (see Suh 1989) that

$$Q(p=q=r=m)=-ig\beta_{11}, \tag{5.15}$$

$$Q(p=m,\,q=r=n)+Q(p=n,\,q=m,\,r=n)=-ig\beta_{12}. \tag{5.16}$$

5.2. *Time-independent angular spectrum models*

The simplest case to be considered of the time-independent model (4.50) may be waves propagating on a constant depth. Neglecting nonlinearity, it becomes

$$A_{s_x}=0, \tag{5.17}$$

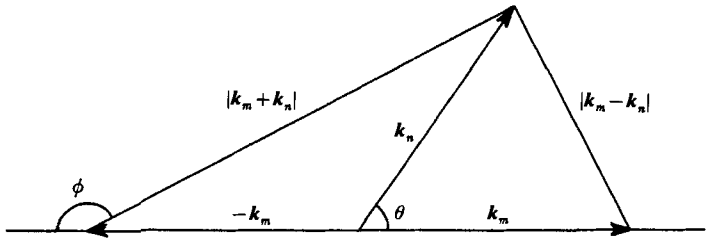

FIGURE 3. Definition of θ and ϕ.

whose solution is

$$A_s(x) = \text{constant} = A_s(0), \tag{5.18}$$

implying the angular spectrum does not change as it propagates on a constant depth.

Another simple case is when waves propagate on a beach with straight and parallel depth contours. For this case, taking the Fourier transform of the mild-slope equation of Berkhoff (1972) in the y-direction, splitting the velocity potential into forward-propagating and backscattered potentials, and neglecting the assumed small backscattered potential, Dalrymple & Kirby (1988) constructed an angular spectrum model given by

$$2(k^2-(s\lambda)^2)^{\frac{1}{2}}CC_g\Phi^+_{s_x}-2\mathrm{i}(k^2-(s\lambda)^2)\,CC_g\Phi^+_s+[(k^2-(s\lambda)^2)^{\frac{1}{2}}CC_g]_x\Phi^+_s=0, \tag{5.19}$$

where the superscript + denotes the forward-propagating component of the wave potential Φ in the mild-slope equation. After substituting for Φ^+_s by

$$\Phi^+_s = A_s\exp\left[\mathrm{i}\int^x (k^2-(s\lambda)^2)^{\frac{1}{2}}\,\mathrm{d}x\right], \tag{5.20}$$

equation (5.19) becomes

$$\frac{(k^2-(s\lambda)^2)^{\frac{1}{2}}}{k}C_gA_{s_x}+\frac{[(k^2-(s\lambda)^2)^{\frac{1}{2}}CC_g]_x}{2\omega}A_s=0, \tag{5.21}$$

which can be obtained by linearizing (4.50) on straight and parallel contours. Thus, (4.50) on straight and parallel contours is the nonlinear extension of Dalrymple & Kirby's wide-angle wave propagation model.

Dalrymple & Kirby's model was extended to the case of irregular bathymetry by Dalrymple *et al.* (1989) in the following form:

$$2(\bar{k}^2-(s\lambda)^2)^{\frac{1}{2}}\tilde{\Phi}^+_{s_x}-2\mathrm{i}(\bar{k}^2-(s\lambda)^2)\,\tilde{\Phi}^+_s+[(\bar{k}^2-(s\lambda)^2)^{\frac{1}{2}}]_x\tilde{\Phi}^+_s+\mathrm{i}\bar{k}^2F_s[\nu^2F^{-1}(\tilde{\Phi}^+_m)]=0, \tag{5.22}$$

where $\tilde{\Phi}=(CC_g)^{\frac{1}{2}}\Phi$ and again the superscript + denotes the forward-propagating wave. Instead of using a laterally averaged depth they used an averaged wavenumber

$$\bar{k}^2=\frac{1}{l}\int_0^l k_c^2\,\mathrm{d}y, \tag{5.23}$$

where

$$k_c^2=k^2-\frac{\nabla^2(CC_g)^{\frac{1}{2}}}{(CC_g)^{\frac{1}{2}}}, \tag{5.24}$$

so ν in (5.22) defined by

$$\nu^2(x,y)=1-\frac{k_c^2}{\bar{k}^2} \tag{5.25}$$

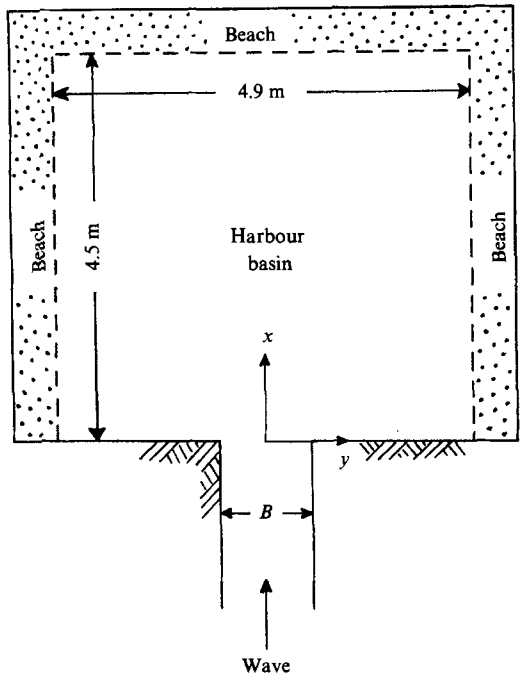

FIGURE 4. Layout of the wave basin in the experiments of Pos & Kilner (1987).

is different from ν in the present study (cf. equation (3.9)) even though both of them represent lateral depth variation. The last term in (5.22) representing wave diffraction due to the interaction between surface wave and lateral bottom variation is replaced by more complicated wave–bottom interaction terms in (4.50), which, in one of the numerical examples in the next section, will be proved to make the present model outperform the Dalrymple *et al.* model.

6. Numerical examples

In order to test the capability of the model for various physical phenomena such as combined refraction–diffraction and nonlinearity, we apply the time-independent model (4.54) to several different water-wave problems for which experimental data are available These include wave diffraction through a breakwater gap and wave focusing behind submerged shoals.

6.1. *Wave diffraction behind a breakwater gap*

The problem of breakwater-gap wave diffraction is important for studying calmness in a breakwater harbour. The experiments of Pos & Kilner (1987) show that linear theory overpredicts wave heights in the open region behind the gap, but underpredicts them in the shadow zones. We apply our nonlinear model to this problem to examine the effect of nonlinearity.

The wave basin used in the Pos & Kilner experiment consists of two impermeable shore-attached breakwaters lying on the y-axis seaward ends of which are extended offshore by jetties separated by a distance B, as shown in figure 4. The wave propagating in the positive x-direction between the jetties is diffracted into the basin. In order to investigate the pure diffraction without distortion of the diffracted wave

field by reflection from the circumferential beaches, they used a photogrammetric wave height measurement technique. Some uncertainties associated with this technique are discussed later.

Six tests of various gap widths and wave characteristics were carried out in the experiments of Pos & Kilner. Here we test our model for only one case for which detailed measurement data along a cross-section are provided in their paper. The constant water depth is 0.125 m. The period and amplitude of the incident wave are 0.67 s and 2.775 cm, respectively. The wavelength, L, computed by linear theory is 0.604 m and the gap width, B, is 0.99 m, so that $B/L = 1.64$.

Since a laterally periodic boundary condition is assumed in the present model, in order to assure negligible effects of the side gaps on the gap being modelled, the width of the model domain should be large compared with the gap width. The model width is taken as sixteen wavelengths so that the ratio of the gap width to the breakwater length is 0.1025. The initial condition is given by the Kirchhoff condition on Φ_x^+ along the breakwater, i.e.

$$\Phi_x^+(0,y) = \begin{cases} \mathrm{i}kA_0, & |y| < \frac{1}{2}B, \\ 0, & |y| > \frac{1}{2}B, \end{cases} \tag{6.1}$$

where Φ^+ is the velocity potential in Dalrymple & Kirby equation (5.19) and A_0 is the initial amplitude assumed to be constant at the gap. $\Phi_{s_x}^+(0)$ is obtained by an FFT of (6.1), and then $\Phi_s^+(0)$ is computed by

$$\Phi_{s_x}^+(0) = \mathrm{i}(k^2-(s\lambda)^2)^{\frac{1}{2}}\Phi_s^+(0), \tag{6.2}$$

which is the reduced form of (5.19) on a constant depth. Finally $A_s'(0) = A_s(0) = \Phi_s^+(0)$ by equations (4.52) and (5.20).

Angular spectrum models using the Fourier transform technique have, in principle, infinite order of accuracy, if the solution is smooth (see Osher 1984). However, the situation changes drastically when discontinuities are present as in equation (6.1). Gibbs phenomenon occurs near the discontinuities and high-frequency oscillations pollute the solution globally since we use a finite Fourier transform in practice. Several smoothing techniques have been used to eliminate this deterioration. The simplest way is to merely set to zero all of the wavenumber spectrum beyond a prescribed magnitude. A slightly more elegant technique is to utilize a low-pass filter which consists of an exponential cut-off of high wavenumbers (e.g. Majda, McDonough & Osher 1978). However, by using this kind of smoothing technique, we loose the most advantageous feature of our model in which the waves propagating at large angles from the predominant wave direction are carried by the high wavenumber components.

Another way to resolve the high-frequency oscillation is to weight-average the solution in the physical domain rather than in the Fourier domain, see, for example, Gottlieb, Lustman & Orszag (1981). In this numerical example, we apply a 5-point averaging in the y-direction to the final solution $A(x,y)$. A 5-point averaging in general has the following form:

$$\bar{A}_j = \alpha A_{j-2} + \beta A_{j-1} + \gamma A_j + \beta A_{j+1} + \alpha A_{j+2}, \tag{6.3}$$

in which the subscripts denote the location in the y-direction (e.g. $A_j = A(x, j\Delta y)$), $2(\alpha+\beta)+\gamma = 1$ and usually $\gamma > \beta > \alpha > 0$. Applying this averaging to the complex solution $A(x,y)$ smooths not only its magnitude but also its phase. However, we want to smooth the magnitude of the solution in a row with its phase unchanged. For this

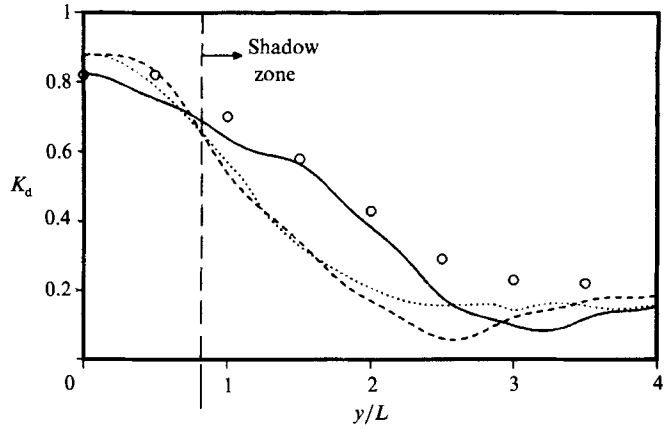

FIGURE 5. Comparison of the model results against the experimental data of Pos & Kilner (1987) in terms of diffraction coefficient (K_d). ○, Experiment; ·····, Penney & Price solution; ---, linear model; ——, nonlinear model.

purpose, we develop the following smoothing procedure. First, the averaged magnitude of the solution at the jth point is calculated by

$$\overline{|A_j|} = \alpha|A_{j-2}| + \beta|A_{j-1}| + \gamma|A_j| + \beta|A_{j+1}| + \alpha|A_{j+2}|. \tag{6.4}$$

The actual smoothed solution is then calculated by

$$\bar{A}_j = \frac{\overline{|A_j|}}{|A_j|} A_j. \tag{6.5}$$

Note that this smoothing is applied to the final solution so that the smoothing effect does not enter the model during the computation of the angular spectrum. In this computation, $\alpha = 0.1$, $\beta = 0.2$, and $\gamma = 0.4$ were used.

The computational results of the present model (both linear and nonlinear) are presented in figure 5 along with the experimental data in terms of diffraction coefficient across the cross-section at $x/L = 3$. The solution of Penney & Price (1952) is also presented for comparison with the linear model result. Since the problem is symmetric about the x-axis, only the right half is presented. As expected, the nonlinear model predicts smaller wave height in the open region and larger wave height in the shadow zone compared with the linear model results, giving better agreement with the experimental data than the linear model.

The nonlinear model underpredicts the measurements throughout the cross-section, and the linear model also provides severe underprediction except at the centreline where it slightly overpredicts the measurement. In the experiments of Pos & Kilner, the photographs of the wave field were taken when the first wavefront arrived at the toe of the backwall beach to avoid the contamination of the diffractive wave field by waves reflected from the beaches. By this time, however, the area near the gap would most likely have been contaminated by wave reflection from the sidewall beaches since the distances from the gap to the sidewall beaches are only about half of that from the gap to the backwall beach. Another question in their experiments is whether the wave field in the basin had reached a steady state at the instant when the photograph was taken, as it is known that there are modulations in wave amplitude at the leading edge of transient wavetrains. Upwave reflection in the entrance channel, owing to the abrupt channel transition, may also contribute to

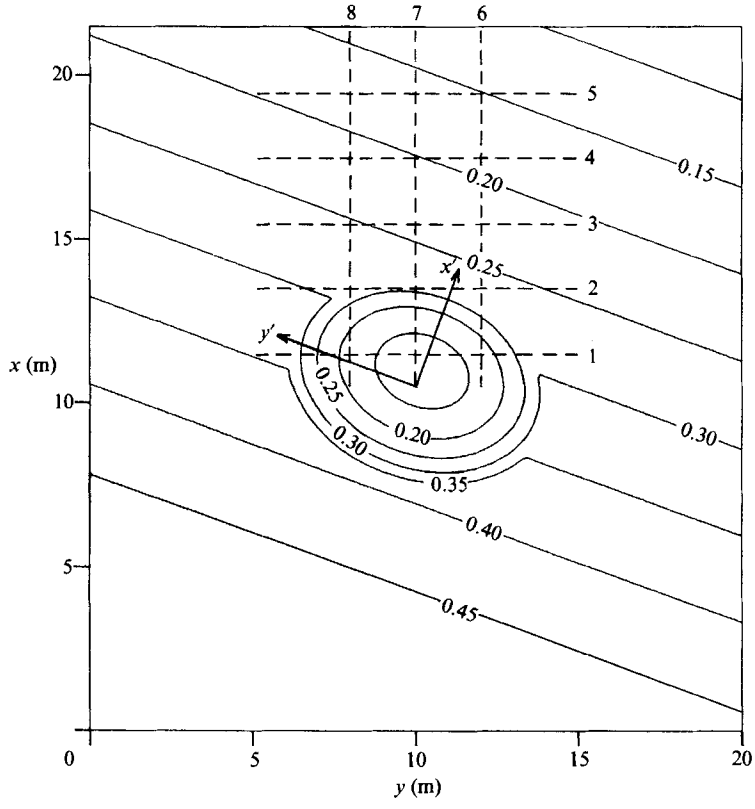

FIGURE 6. Bathymetry of the computational domain for the experiment of Berkhoff *et al.* (1982). Dashed lines indicate the transects of wave measurement.

the discrepancy between the measurement and model prediction. Assuming perfectly-reflecting sidewalls, Dalrymple (1989) estimated the reflection at 6%. This upwave reflection and its re-reflection from the wavemaker will produce partial standing waves in the entrance channel. It is not clear if this was taken into consideration in their experiment.

6.2. *Wave focusing behind an elliptic shoal on a sloping beach*

For the purpose of testing the model for the prediction of wave deformation on an irregular bathymetry, we have chosen the experiment reported in Berkhoff, Booij & Radder (1982). The experimental bathymetry consists of an elliptic shoal situating on a sloping beach with a slope 1:50. The slope rises from a region of constant depth $h = 0.45$ m, and the entire slope is rotated at an angle of 20° from the y-axis as shown in figure 6, where the solid lines indicate bottom contours and the dashed lines are the transects along which data from the experiment of Berkhoff *et al.* are available. The details of the geometry of the shoal in the present coordinate system are referred to Dalrymple *et al.* (1989). The wave propagating in the positive *x-direction at* $x =$ 0 has 2.32 cm amplitude and 1 s period.

The graphical comparison between the model results and the measurements along the transects 1–8 is given in figure 7, showing that the nonlinearity is important at the transects 4 and 5 where the wave has passed through the caustic cusp. Here we present a more quantitative comparison using a statistical parameter proposed by

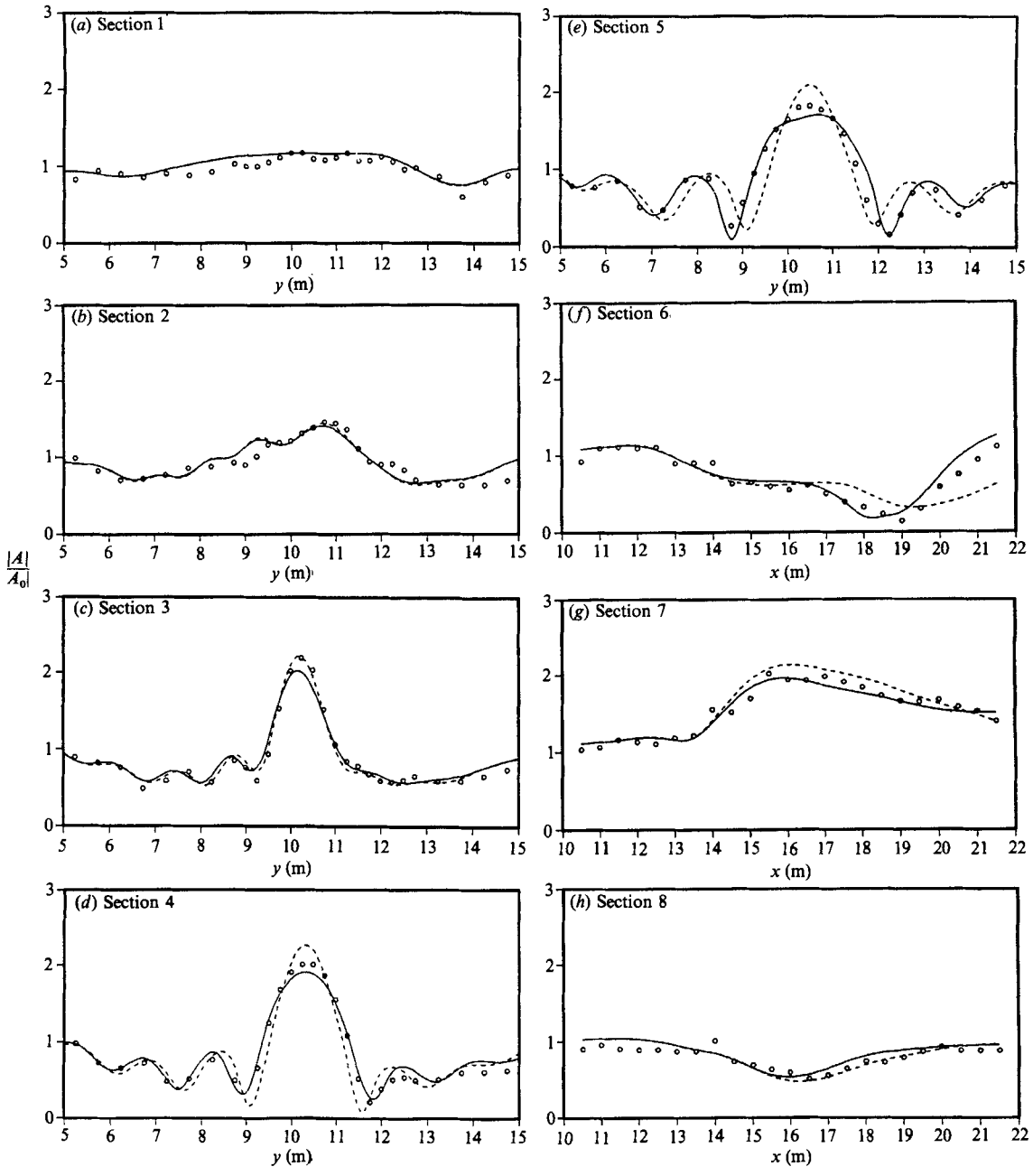

FIGURE 7. Comparison of the model results against the experimental data of Berkhoff *et al.* (1982) in terms of normalized amplitude with respect to incident amplitude. ○, Experiment; ---, linear model; ——, nonlinear model.

Section no.	N	Linear			Nonlinear		
		Present	Dalrymple *et al.*	Parabolic	Present	Dalrymple *et al.*	Parabolic
1	28	0.897	0.852	0.918	0.897	0.913	0.928
2	28	0.953	0.847	0.934	0.952	0.945	0.973
3	28	0.995	0.946	0.975	0.988	0.986	0.983
4	27	0.976	0.898	0.935	0.993	0.991	0.993
5	28	0.944	0.706	0.854	0.988	0.982	0.990
6	23	0.883	0.472	0.645	0.969	0.970	0.988
7	23	0.972	0.699	0.891	0.981	0.954	0.985
8	23	0.930	0.844	0.875	0.901	0.796	0.951
Total	208	0.973	0.867	0.933	0.987	0.982	0.990

TABLE 1. Indices of agreement for comparing the numerical model results against the measurements for the experiment of Berkhoff *et al.* (1982)

Willmott (1981). As a measure of the degree to which a model's predictions are error-free, he introduced a dimensionless quantity, d, as an index of agreement

$$d = 1 - \frac{\sum_{i=1}^{N} (P_i - O_i)^2}{\sum_{i=1}^{N} (|P_i - \bar{O}| + |O_i - \bar{O}|)^2}, \tag{6.6}$$

where $\bar{O}$ is the mean of the observed variates O_i, and P_i, $i = 1$ to N, are the predicted variates. The values for d vary between 0 and 1.0, where 1.0 indicates perfect agreement between observation and prediction, and 0 connotes complete disagreement.

The indices of agreement computed for each transect in figure 6 and for total measurement points are given in table 1, in which the results of the Dalrymple *et al.* model (5.22) and the parabolic model of Kirby & Dalrymple (1983) are also presented for comparison. For all the transects, the present linear model gives much better agreement with the measurements than the Dalrymple *et al.* linear model, probably because the wave–bottom interaction is represented in a more elaborate manner in the present model. The present linear model also outperforms the linear parabolic model. On transects 2, 3 and 8, the present linear model gives even better agreement than the nonlinear model. Though the nonlinear parabolic model performs slightly better than the other nonlinear models, the indices of agreement do not show big differences among the nonlinear models and are close to 1.0, indicating that all the nonlinear models work quite well.

Another measure to compare the performance of numerical models may be the computing time, though it is not a critical factor owing to the development of high-speed computers. The amounts of CPU time and the grid sizes of each model are given in table 2. The grid sizes were taken differently from one model to another considering the accuracy and stability of the solution. The computer used is a PRIME 9955 Minicomputer with 16 megabytes RAM and a virtual memory operating system. There is no difference in computing time between the linear and nonlinear versions of the parabolic model. The difference is small between the linear and nonlinear versions of the Dalrymple *et al.* model. The computing time of the present nonlinear model, however, increases greatly compared with that of the linear

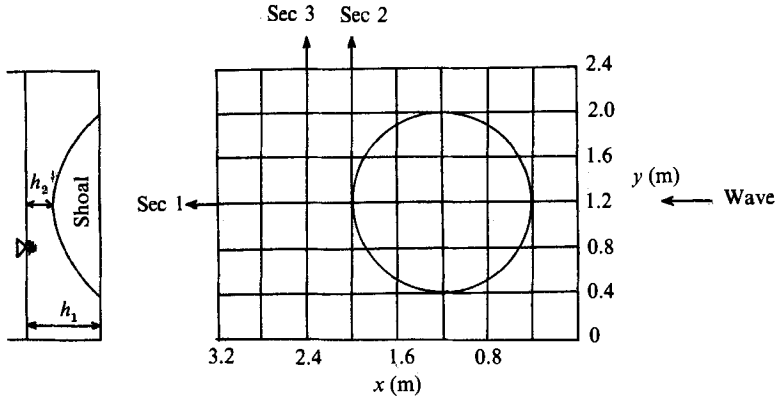

FIGURE 8. Geometry of the computational domain for the experiment of Ito & Tanimoto (1972).

	Present	Dalrymple *et al.*	Parabolic
Linear	25 s	1 min 29 s	1 min 22 s
Nonlinear	11 min 53 s	1 min 53 s	1 min 22 s
Δx	0.5 m	0.1 m	0.25 m
Δy	0.3125 m	0.3125 m	0.25 m

TABLE 2. Comparison of CPU time in modelling the experiment of Berkhoff *et al.* (1982)

model owing to the computation of the cubic nonlinear terms involving triple summations. The present linear model gives the best result (cf. table 1) with the least computing time but its nonlinear version takes the greatest computing time.

6.3. *Wave focusing behind a circular shoal resting on a flat bottom*

The most advantageous feature of the angular spectrum model is that it permits solution by a marching method like the parabolic model but is valid for waves propagating at large angles from the assumed propagation direction. For the purpose of testing the model for waves propagating over an irregular bathymetry at large angles of incidence, we have chosen the experiment reported by Ito & Tanimoto (1972). Their experimental bathymetry consists of a circular shoal resting on a flat bottom. A monochromatic wavetrain propagates over the shoal, and wave focusing occurs behind the shoal. Owing to the axisymmetry of the circular shoal, the wave focusing pattern behind the shoal should be independent of the angle of incidence, if the model predicts it 'correctly'.

The geometry of Ito & Tanimoto experiment is shown in figure 8. The water depth on the flat bottom $h_1 = 0.15$ m, and the water depth in the shoal region is described by

$$h = h_2 + 0.15625\,[(x-1.2)^2 + (y-1.2)^2], \tag{6.7}$$

where $h_2 = 0.05$ m is the depth at the shoal crest. A monochromatic wavetrain with 1.04 cm wave height and 0.511 s period enters the domain at $\theta_0 = 0°$. For the three different sections indicated in figure 8, data from the experiment of Ito & Tanimoto are available. Comparison with the model results along these sections are shown in figure 9(*a–c*) in terms of normalized wave amplitude with respect to the incident

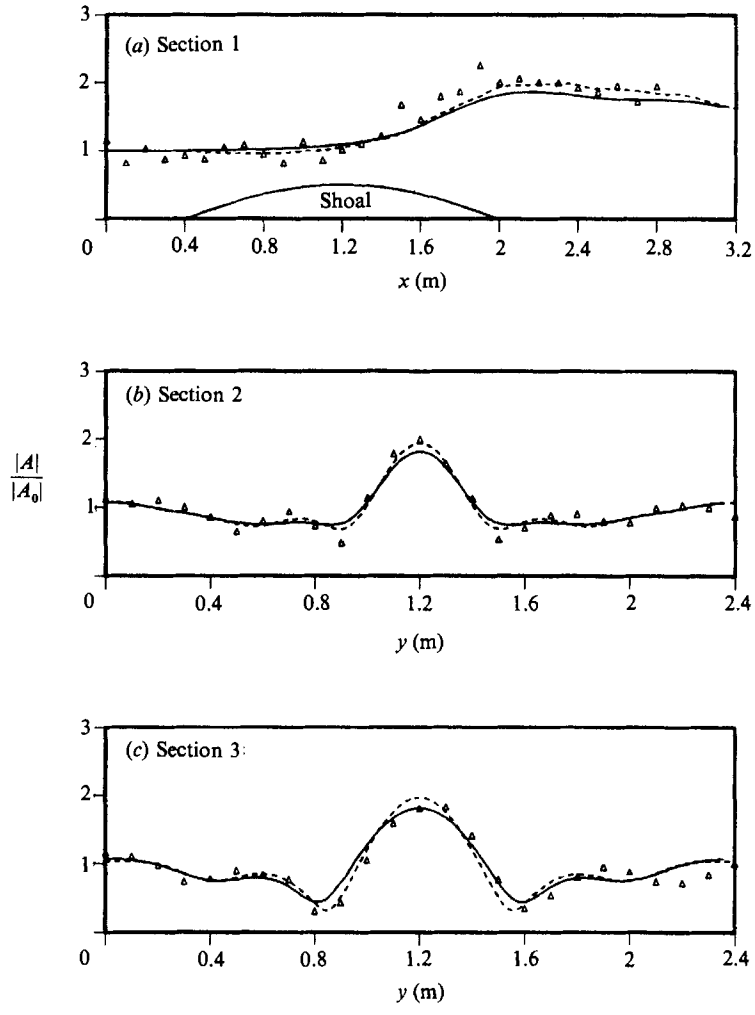

FIGURE 9. Comparison of the model results against the experimental data by Ito & Tanimoto (1972) in terms of normalized wave amplitude with respect to the incident amplitude. △, Experiment; ——, present nonlinear model; – – –, nonlinear parabolic model.

amplitude. In each figure, nonlinear results of the present model are given by solid lines, while triangles indicate measured data points. The results of the large-angle parabolic model of Kirby (1986) are also given by dashed lines. This model uses the minimax approximation to obtain better accuracy for waves propagating at large angles. Both models predict the measurement reasonably well.

In order to test the model for a large angle of incidence, the flat bottom in figure 8 is extended to $y \approx 4.8$ m and the wave focusing is modelled for two different incident angles: $\theta_0 = 45°$ and $\theta_0 = 60°$. To satisfy the lateral periodicity of the wave field, the model width is taken to be an integer multiple of the lateral wavelength of the incident wave field but close to 4.8 m. Otherwise the discontinuity of the initial wave field at the side boundaries propagates into the domain, contaminating the solution. A qualitative comparison with the results of normal incidence can be made by comparing the contour maps of wave amplitude or instantaneous surface elevation for each incident angle. For a more quantitative comparison, the variation

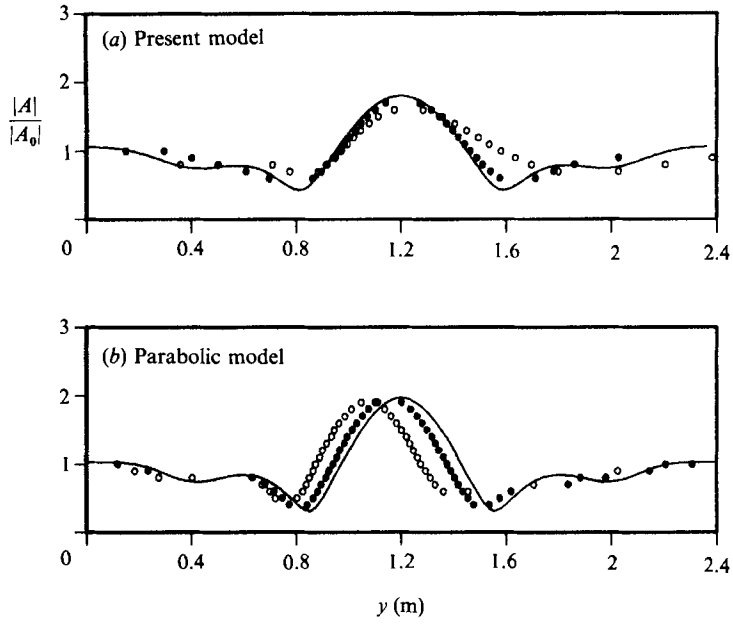

FIGURE 10. Comparison of the model results of $\theta_0 = 45°$ and $\theta_0 = 60°$ against those of normal incidence in terms of normalized wave amplitude with respect to the incident amplitude at section 3 indicated in figure 8: (*a*) present model, (*b*) parabolic model; ——, normal incidence; ●, 45°; ○, 60°.

of the normalized amplitude along the section 3 (in figure 8) for different angles of incidence is plotted in figure 10. The values of normal incidence are indicated by a solid line, and the solid and open circles indicate the values at $\theta_0 = 45°$ and 60°, respectively, which were obtained by digitization from the contour maps of normalized amplitude. A similar figure for the parabolic model of Kirby (1986) is also presented.

The results of the present model for $\theta_0 = 45°$ closely follow those of normal incidence except near the right depression, whereas for $\theta_0 = 60°$ the disagreement is more pronounced, especially on the right-hand side of the caustic cusp. The overall shapes of the results of the parabolic model for $\theta_0 = 45°$ and 60° are very similar to that for normal incidence, but they are shifted to the left, indicating that the focused wave fields for $\theta_0 = 45°$ and 60° rotate towards the positive x-direction. The shift becomes severe with increasing angle of incidence, and it is more prominent on the right-hand side of the caustic cusp.

Dalrymple *et al.* (1989) have presented a simple theoretical analysis regarding the accuracy of their angular spectrum model in terms of lateral depth variation and wave propagation angle, concluding that in order for their model to be accurate for a large angle of incidence, the lateral depth variation should be small. A similar analysis can be applied to the wave–bottom interaction terms involving ν in the present model (4.54). The height of the shoal in the above example is $\frac{2}{3}$ of the water depth on the flat bottom (unusually high considering the normal situation in real cases). In order to examine the effects of the magnitude of the lateral bottom variation, we have tested the model for a shoal having half the height of the shoal shown in figure 8 (i.e. $h_2 = 0.1$ m in equation (6.7)). Figure 11 presents results similar to those presented in figure 10 for smaller shoal height. The results for $\theta_0 = 45°$

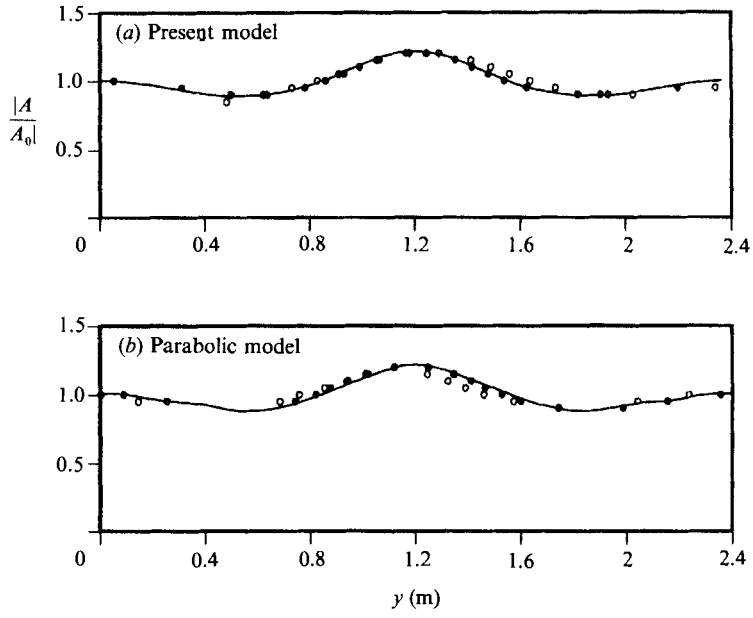

FIGURE 11. Same as figure 10 for the results of the test with smaller shoal height.

almost exactly match those of normal incidence in both models and those for $\theta_0 = 60°$ also give good agreement with the normal incidence.

There are some other problems associated with the large-angle propagation in this example. First, the constant-depth region before the shoal ($x < 0.4$ m in figure 8) should be affected by the presence of the shoal if a large angle of incidence is modelled, but this is not detected by the model since it does not include backscattering waves. Secondly, the assumption of lateral periodicity makes the effect of the imaginary upwave shoal appear in the domain to be modelled when a wave is incident at a large angle. The latter problem can be resolved by taking a wider domain.

7. Conclusions

The present study has developed an angular spectrum model for predicting the transformation of Stokes waves due to refraction, diffraction, shoaling and nonlinear wave interactions in water of varying depth but free of ambient currents. The bottom slope is assumed to be $O(\epsilon^2)$ and the deviation of the actual depth from the laterally-averaged depth is assumed to be $O(\epsilon)$ of the laterally-averaged depth. In order for the model to be valid for the case in which waves propagate at large angles from the x-direction, the second assumption should not be violated.

Through the example for wave focusing behind an elliptic shoal on a sloping beach, the present linear model has proved to predict the wave transformation on an irregular bathymetry much better than the linear model of Dalrymple *et al.* (1989), probably owing to the more elaborate expressions for the wave–bottom interaction in the present model. The nonlinear models, however, did not show big differences between each other and both predicted the measurement reasonably well. The advantages of the Dalrymple *et al.* nonlinear model are that it can be applied over the entire range of water depths and that the effects of ambient current can be included easily by modifying the dispersion relationship. The advantage of the

present model is that it can be extended to a random directional wave field including the nonlinear interaction among the waves with different frequencies as in Suh (1989).

This work is partly a result of research sponsored by NOAA Office of Sea Grant, Department of Commerce, under Grand no. NA86AADSG040. J.T.K. received support from the Office of Naval Research, contracts N00014-86-K-0790 and N00014-89-J-1717. The US Government is authorized to produce and distribute reprints for governmental purposes, notwithstanding any copyright notation that may appear herein.

Appendix. Summary of the forcing terms

The forcing terms in the boundary-value problems (3.14)–(3.17) are summarized as follows:

$$F_1 = 0, \tag{A 1}$$

$$F_2 = -\phi_{1_{xx_1}} - \phi_{1_{x_1x}}, \tag{A 2}$$

$$F_3 = -\phi_{1_{x_1x_1}} - \phi_{1_{xx_2}} - \phi_{1_{x_2x}} - \phi_{2_{xx_1}} - \phi_{2_{x_1x}}, \tag{A 3}$$

$$G_1 = 0, \tag{A 4}$$

$$G_2 = -2\phi_{1_{tt_1}} - \eta_1\phi_{1_{ttz}} - g\eta_1\phi_{1_{zz}} - 2(\phi_{1_x}\phi_{1_{xt}} + \phi_{1_y}\phi_{1_{yt}} + \phi_{1_z}\phi_{1_{zt}}), \tag{A 5}$$

$$\begin{aligned} G_3 = {} & -2\phi_{2_{tt_1}} - 2\phi_{1_{tt_2}} - \phi_{1_{t_1t_1}} - \eta_1\phi_{2_{ttz}} - 2\eta_1\phi_{1_{tt_1z}} - \eta_2\phi_{1_{ttz}} \\ & - g\eta_1\phi_{2_{zz}} - g\eta_2\phi_{1_{zz}} - \tfrac{1}{2}\eta_1^2\phi_{1_{ttzz}} - \tfrac{1}{2}g\eta_1^2\phi_{1_{zzz}} \\ & - \phi_{1_x}^2\phi_{1_{xx}} - \phi_{1_y}^2\phi_{1_{yy}} - \phi_{1_z}^2\phi_{1_{zz}} \\ & - 2(\phi_{1_x}\phi_{1_y}\phi_{1_{xy}} + \phi_{1_x}\phi_{1_z}\phi_{1_{xz}} + \phi_{1_y}\phi_{1_z}\phi_{1_{yz}}) \\ & - 2(\phi_{1_x}\phi_{2_{xt}} + \phi_{1_x}\phi_{1_{xt_1}} + \phi_{2_x}\phi_{1_{xt}} + \phi_{1_{x_1}}\phi_{1_{xt}}) \\ & - 2(\phi_{1_y}\phi_{2_{yt}} + \phi_{1_y}\phi_{1_{yt_1}} + \phi_{2_y}\phi_{1_{yt}}) - 2(\phi_{1_z}\phi_{2_{zt}} + \phi_{1_z}\phi_{1_{zt_1}} + \phi_{2_z}\phi_{1_{zt}}) \\ & - 2\eta_1(\phi_{1_{xt}}\phi_{1_{xz}} + \phi_{1_x}\phi_{1_{xtz}} + \phi_{1_{yt}}\phi_{1_{yz}} + \phi_{1_y}\phi_{1_{ytz}} + \phi_{1_{zt}}\phi_{1_{zz}} + \phi_{1_z}\phi_{1_{ztz}}), \end{aligned} \tag{A 6}$$

$$H_1 = 0, \tag{A 7}$$

$$H_2 = -\phi_{1_{t_1}} - \eta_1\phi_{1_{tz}} - \tfrac{1}{2}(\phi_{1_x}^2 + \phi_{1_y}^2 + \phi_{1_z}^2), \tag{A 8}$$

$$B_1 = 0, \tag{A 9}$$

$$B_2 = -\bar{h}\mu\phi_{1_{zz}}, \tag{A 10}$$

$$B_3 = -\phi_{1_x}h_{x_2} - \phi_{1_y}h_{y_2} - \bar{h}\mu\phi_{2_{zz}} - \tfrac{1}{2}\bar{h}^2\mu^2\phi_{1_{zzz}}. \tag{A 11}$$

REFERENCES

BENNEY, D. J. & NEWELL, A. C. 1967 The propagation of nonlinear wave envelopes. *J. Math. Phys.* **46**, 133–139.

BENNEY, D. J. & ROSKES, G. J. 1969 Wave instabilities. *Stud. Appl. Maths* **48**, 377–385.

BERKHOFF, J. C. W. 1972 Computation of combined refraction–diffraction. *Proc. 13th Intl Conf. Coastal Engng, ASCE, Vancouver*, pp. 471–490.

BERKHOFF, J. C. W., BOOIJ, N. & RADDER, A. C. 1982 Verification of numerical wave propagation models for simple harmonic linear waves. *Coastal Engng.* **6**, 255–279.

BOOKER, H. G. & CLEMMOW, P. C. 1950 The concept of an angular spectrum of plane waves, and its relation to that of polar diagram and aperture distribution. *Proc. Inst. Elect. Engrs*, part 3, **97**, 11–17.

CLEMMOW, P. C. 1986 *The Plane Wave Spectrum Representation of Electromagnetic Fields*, Pergamon. 185 pp.

DALRYMPLE, R. A. 1989 Water waves past abrupt channel transitions. *Appl. Ocean Res.* (In Press.)

DALRYMPLE, R. A. & KIRBY, J. T. 1988 Models for very wide-angle water waves and wave diffraction. *J. Fluid Mech.* **192**, 33–50.

DALRYMPLE, R. A., SUH, K. D., KIRBY, J. T. & CHAE, J. W. 1989 Models for very wide-angle water waves and wave diffraction. Part 2. Irregular bathymetry. *J. Fluid Mech.* **201**, 299–322.

DAVEY, A. & STEWARTSON, K. 1974 On three-dimensional packets of surface waves. *Proc. R. Soc. Lond.* A **338**, 101–110.

DJORDJEVIĆ, V. D. & REDEKOPP, L. G. 1978 On the development of packets of surface gravity wave moving over an uneven bottom. *Z. angew. Math. Phys.* **29**, 950–962.

GABOR, D. 1961 Light and information. In *Progress in Optics* (ed. E. Wolf), vol. 1. North-Holland.

GOTTLIEB, D., LUSTMAN, L. & ORSZAG, S. A. 1981 Spectral calculations of one-dimensional inviscid compressible flows. *SIAM J. Sci. Stat. Comput.* **2**, 296–310.

ITO, Y. & TANIMOTO, K. 1972 A method of numerical analysis of wave propagation: Application to wave diffraction and refraction. *Proc. 13th Intl Conf. Coastal Engng, ASCE, Vancouver*, pp. 503–522.

KIRBY, J. T. 1986 Rational approximations in the parabolic equation method for water waves. *Coastal Engng.* **10**, 355–378.

KIRBY, J. T. & DALRYMPLE, R. A. 1983 A parabolic equation for the combined refraction–diffraction of Stokes waves by mildly varying topography. *J. Fluid Mech.* **136**, 453–466.

KIRBY, J. T. & DALRYMPLE, R. A. 1986 An approximate model for nonlinear dispersion in monochromatic wave propagation models. *Coastal Engng* **9**, 545–561.

LONGUET-HIGGINS, M. S. 1962 Resonant interactions between two trains of gravity waves. *J. Fluid Mech.* **12**, 321–332.

MAJDA, A., MCDONOUGH, J. & OSHER, S. 1978 The Fourier method for nonsmooth initial data. *Math. Comput.* **32**, 1041–1081.

OSHER, S. 1984 Smoothing for spectral methods. In *Spectral Methods for Partial Differential Equations* (ed. R. G. Voigt, D. Gottlieb & M. Y. Hussaini). SIAM.

PENNEY, W. G. & PRICE, A. T. 1952 The diffraction theory of sea waves and the shelter afforded by breakwaters. *Phil. Trans. R. Soc. Lond.* A **244**, 236–253.

PHILLIPS, O. M. 1960 On the dynamics of unsteady gravity waves of finite amplitude. Part 1. The elementary interactions. *J. Fluid Mech.* **9**, 193–217.

POS, J. D. & KILNER, F. A. 1987 Breakwater gap wave diffraction: An experimental and numerical study. *J. Waterway Port Coast. Ocean Engng* **113**, 1–21.

RATCLIFFE, J. A. 1956 Some aspects of diffraction theory and their application to the ionosphere. In *Reports on Progress in Physics*, vol. 19, (ed. A. C. Strickland). The Physical Society, London.

ROSKES, G. J. 1976*a* Some nonlinear multiphase interactions. *Stud. Appl. Maths* **55**, 231–238.

ROSKES, G. J. 1976*b* Nonlinear multiphase deep-water wavetrains. *Phys. Fluids.* **19**, 1253–1254.

SHARMA, J. N. & DEAN, R. G. 1979 Development and evaluation of a procedure for simulating a random directional second order sea surface and associated wave forces. *Ocean Engng Rep.* 20. University of Delaware.

STAMNES, J. J. 1986 *Waves in Focal Regions.* Bristol: Adam Hilger. 600 pp.

STAMNES, J. J., LØVHAUGEN, O., SPJELKAVIK, B., MEI, C. C., LO, E. & YUE, D. K. P. 1983 Nonlinear focusing of surface waves by a lens – theory and experiment. *J. Fluid Mech.* **135**, 71–94.

SUH, K. D. 1989 Angular spectrum models for propagation of weakly nonlinear surface gravity waves in water of varying depth. PhD dissertation, University of Delaware.

WILLMOTT, C. J. 1981 On the validation of models. *Phys. Geog.* **2**, 184–194.

YUE, D. K.-P. & MEI, C. C. 1980 Forward diffraction of Stokes waves by a thin wedge. *J. Fluid Mech.* **99**, 33–52.